

Cross-over from trion-hole to exciton-polaron in n -doped semiconductor quantum wells

Yia-Chung Chang^{1,2*} and Shiue-Yuan Shiau^{1,3}, Monique Combescot⁴

¹ *Research Center for Applied Sciences, Academic Sinica, Taipei, 11529 Taiwan*

² *Department of Physics, National Cheng Kung University, Tainan, 701 Taiwan*

³ *Physics Division, National Center for Theoretical Sciences, Hsinchu, 30013, Taiwan and*

⁴ *Sorbonne Université, CNRS, Institut des NanoSciences de Paris, 75005-Paris, France*

(Dated: November 1, 2018)

We present a theoretical study of photo-absorption in n -doped two-dimensional (2D) and quasi-2D semiconductors that takes into account the interaction of the photocreated exciton with Fermi-sea (FS) electrons through (i) Pauli blocking, (ii) Coulomb screening, and (iii) excitation of FS electron-hole pairs—that we here restrict to one. The system we tackle is thus made of one exciton plus zero or one FS electron-hole pair. At low doping, the system ground state is predominantly made of a “trion-hole”—a trion (two opposite-spin electrons plus a valence hole) weakly bound to a FS hole—with a small exciton component. As the trion is poorly coupled to photon, the intensity of the lowest absorption peak is weak; it increases with doping, thanks to the growing exciton component, due to a larger coupling between 2-particle and 4-particle states. Under a further doping increase, the trion-hole complex is less bound because of Pauli blocking by FS electrons, and its energy increases. The lower peak then becomes predominantly due to an exciton dressed by FS electron-hole pairs, that is, an exciton-polaron. As a result, the absorption spectra of n -doped semiconductor quantum wells show two prominent peaks, the nature of the lowest peak turning from trion-hole to exciton-polaron under a doping increase. Our work also nails down the physical mechanism behind the increase with doping of the energy separation between the trion-hole peak and the exciton-polaron peak, even before the anti-crossing, as experimentally observed.

I. INTRODUCTION

Optical spectra associated with excitons in the presence of a Fermi sea (FS) in bulk¹ or quantum well^{2–12} semiconductors have been a subject of great interest for decades. Depending on the doping concentration, the Coulomb interaction between the photocreated exciton and the FS electrons can lead to various exotic complexes that come from the dressing of the exciton by Fermi-sea excitations, *i.e.*, FS electron-hole pairs—the “FS hole” which corresponds to a missing electron in the doped conduction band, being fundamentally different from the valence hole making the exciton. Interestingly, at low doping, a bound state can emerge from the interaction of a trion (two opposite-spin electrons bound to a valence hole) and a FS hole, known as Suris tetron^{10–12}. When the FS contains just one electron, this 4-particle complex reduces to the conventional X^- trion because there is no other hole state for the FS hole to scatter into to possibly form a bound state with the trion through repeated interactions.

Experiments on optical excitation spectra in n -doped II-VI quantum wells (QWs) show two peaks that are commonly associated with the negatively charged trion (X^-) and the exciton (X), separated by an energy that increases steadily with doping concentration^{8–10}. This increase in energy difference contradicts common physical understanding: Indeed, the trion binding should decrease when the doping increases because of the increase of Pauli blocking and the reduction of Coulomb interaction due to screening by the doping electrons. Theoretical studies using many-body Green functions have con-

firmed that absorption spectra should show two prominent peaks, separated by an energy difference that increases with doping^{9–12}. Although the precise nature of these two peaks has not been established, it is clear that they must come from many-body interactions between an exciton and FS electron-hole pairs.

Today, a considerable interest is devoted to these bound complexes that also appear in the photo-absorption spectra of n -doped 2D transition-metal dichalcogenides (TMDs)^{15–18}. In these new 2D materials, excitons and trions have unusually strong bindings due to a strong reduction of the dielectric constant^{19–22} (the trion binding can be as large as 30meV ^{15,26–31}). Strong bindings, along with large binding energy differences, render these materials quite suitable for studying the interplay between excitons and trions under a doping increase, for temperature as high as room temperature.

In a previous work, we have demonstrated the possibility of observing the implausible “trion-polariton” in doped 2D semiconductors when the Fermi sea is spin-polarized¹⁹. In this work, we study the evolution of the photo-absorption spectra in 2D and quasi-2D QWs of III-V and II-VI semiconductors when the doping increases. We show that at low doping, the lowest peak corresponds to a bound “trion-hole”, that is, the ground state of a trion and a FS hole. The higher peak corresponds to the exciton-polaron¹⁴, that is, an exciton dressed by FS electron-hole pairs, which tends to an exciton when the doping goes to zero. While the energies of the trion-hole and the exciton-polaron would eventually cross when the doping increases, Coulomb interactions between them prevent this crossing from happening by producing an

anti-crossing. For higher doping, the lower peak is due to the exciton-polaron and the higher peak due to the trion-hole.

In addition, the exciton encounters a cascade of anti-crossings, at smaller dopings, with the *excited* trion-hole states that are distributed within a swath of energy of the order of the Fermi-sea energy (see Fig. 8). This broadens the higher peak. As a result, the energy separation between the low and high peaks increases not only after the anti-crossing, but, surprisingly, also before the anti-crossing due to the multiple anti-crossings with the excited trion-hole states. This understanding provides a much sought-after explanation for the counterintuitive experimental findings that the separation between the two peaks *always* increases as the doping increases, despite the fact that the binding of the trion with respect to the exciton reduces when the doping increases. At even higher doping, contributions to the exciton-polaron from multiple FS electron-hole pairs become sizable and ultimately lead to Fermi edge singularities¹⁴.

To characterize the system ground state as a function of the Fermi momentum k_F , we show in Fig. 1 the squared amplitudes of the trion-hole and exciton-polaron components of this ground state. For numerical purpose, the exciton-polaron considered here is dressed by zero or one FS electron-hole pair. Two cases are considered: (i) unpolarized FS, and (ii) polarized FS with electron spin opposite to the spin of the photo-created electron. At the cross-over, the ground state has an equal amount of these two components. Before the cross-over, the ground state corresponds to a trion bound to a FS hole, whereas after the cross-over, the ground state leans predominantly toward exciton-polaron. With a_X being the 3D exciton Bohr radius, the cross-over for spin-polarized (unpolarized) FS occurs at $k_F a_X \simeq 0.8$ (0.7) for 2D QW, but at 0.45 (0.4) for quasi-2D GaAs/Al_{0.25}Ga_{0.75} QW with 8nm thickness. This shows that Pauli blocking and Coulomb screening facilitate the transition to exciton-polaron.

To mathematically study the cross-over between trion-hole and exciton-polaron, we use two sets of basis functions: one set is made of one exciton (with its ground and excited levels) in the presence of a rigid FS; the other set is made of one exciton in the presence of one FS electron-hole pair; this basis can also be taken as one trion (with its ground or excited level) with one FS hole. We perform a “configuration-interaction” calculation to allow us to determine not only the ground state but also the excited states of the system. A particular focus is made on the Pauli exclusion principle induced by the Fermi sea, either polarized or unpolarized, and its competition with the formation of the trion-hole complex and exciton-polaron. What fundamentally distinguishes our method from the many-body Green’s function method used in Ref. 10 is that our approach can provide a clear identification of the physical nature in each peak through the wave functions that are involved, an essential point to possibly study the cross-over.

To best understand the effect of Pauli blocking, we first

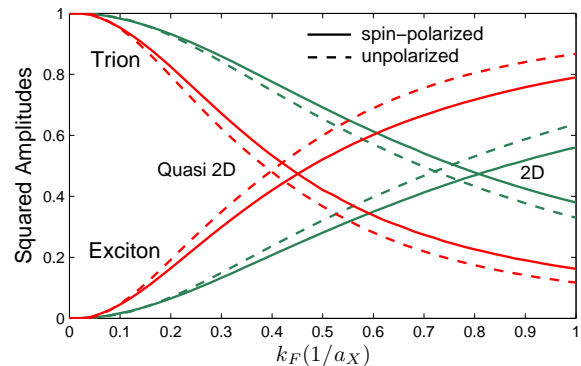


FIG. 1: Squared amplitudes of the trion component and exciton component in the 4-particle ground state for spin-polarized (solid) and unpolarized (dashed) Fermi seas as functions of the Fermi momentum k_F , for 2D (green) and quasi-2D (red) QWs.

study the binding energies of the exciton and trion in the presence of a “frozen” Fermi sea, that is, a FS without any electron-hole excitation, when the exciton is photo-created in a semiconductor QW by the absorption of a circularly-polarized (σ_+) photon; the resulting exciton is then made of a spin-(-1/2) conduction electron and a (+3/2) valence hole. When the Fermi sea is unpolarized, both the exciton and the trion suffer Pauli blocking, which makes their binding energy decrease when the doping increases. When the Fermi sea is fully polarized with spin-(1/2) electrons only, the photo-created exciton does not suffer Pauli blocking, whereas the spin-(1/2) electron of the trion does. In both cases, we find that the lowest peak changes from trion-hole to exciton-polaron when the doping increases, but not at the same doping value.

To tackle this complex system, we use the Rayleigh-Ritz variational method^{32,33} that consists of expanding the bound states we want to determine on a finite set of localized basis functions. We solve the resulting Schrödinger equation within this basis subspace, through a numerical diagonalization. The valence-hole effective mass is taken as infinite; this simplification, which does not affect the existence of bound states, allows reducing the basis functions to products of single-particle wave functions for electrons above the FS and hole in the FS. We have included the reduction of the Coulomb interaction induced by the doped electrons through the Thomas-Fermi screening. To understand the effect of the QW thickness on this cross-over and catch the trend it induces, we have considered 2D and quasi-2D QWs by using an effective Coulomb scattering that varies from $1/q$ to $1/q^2$ when the well thickness increases and which have been shown to give excellent agreement with experiments³.

The paper is organized as follows. In Sec. II, we present the problem. In Sec. III, we introduce the basis functions that we use for the FS hole and the two electrons outside the FS. In Sec. IV and V, we calculate the low-lying ex-

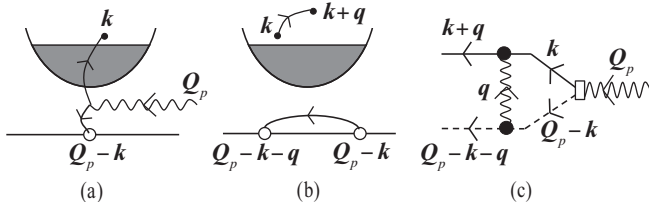


FIG. 2: (a) The absorption of a Q_p photon creates a valence hole ($Q_p - k$) and a conduction electron k outside the FS. (b) Coulomb scattering of the photo-created pair for a frozen FS. Repeated interactions of the pair lead to the formation of an exciton, although weaker because some conduction states are Pauli blocked by the FS. (c) Feynman diagram for processes (a) and (b). Solid line represents conduction electron, dashed line represents valence hole. Squiggly line represents Coulomb interaction.

citon and trion states and their binding energies without and with a frozen FS, either fully polarized or unpolarized. The undoped case is used as a benchmark to show the accuracy of our variational procedure. In Sec. VI, we turn to the trion-hole complex and the exciton-polaron, and study their cross-over. Next, we discuss the consequences on photo-absorption spectra, and we conclude.

II. PHYSICS OF THE PROBLEM

We look for the absorption spectrum of a photon with momentum Q_p in the presence of a Fermi sea that we take as $|F_N\rangle = \prod_{i=1}^N a_{\mathbf{k}_i}^\dagger |v\rangle$ with $|\mathbf{k}_i| \leq k_F$, with $|v\rangle$ denoting the vacuum state. To facilitate the argument, we neglect the particle spin degrees of freedom; they will be introduced in due course. The Fermi golden rule gives the photon absorption spectrum $\mathcal{A}(Q_p)$ through

$$\mathcal{A}(Q_p) \propto \sum_f |\langle f | U_{ph-sc}^\dagger | i \rangle|^2 \delta(E_f - E_i), \quad (1)$$

where $|i\rangle$ and $|f\rangle$ are, respectively, the system eigenstates before and after photo-absorption, their energies being E_i and E_f .

The initial state $|i\rangle$ consists of the photon Q_p with energy $\hbar\omega_{Q_p}$ and the Fermi sea $|F_N\rangle$ with energy \mathcal{E}_N , that is, $|i\rangle = a_{Q_p}^\dagger |F_N\rangle$ with energy $E_i = \hbar\omega_{Q_p} + \mathcal{E}_N$. When acting on $|i\rangle$, the photon-semiconductor coupling U_{ph-sc}^\dagger destroys the photon Q_p and creates a pair of conduction electron and valence hole with same total momentum (see Fig. 2(a)); so,

$$U_{ph-sc}^\dagger |i\rangle = \Omega \sum_{\mathbf{k}} a_{\mathbf{k}}^\dagger b_{-\mathbf{k}+Q_p}^\dagger |F_N\rangle \equiv \Omega |i'\rangle, \quad (2)$$

where Ω is the vacuum Rabi coupling and $a_{\mathbf{k}}^\dagger$ ($b_{\mathbf{k}}^\dagger$) creates a free conduction electron (valence hole) with momentum \mathbf{k} . We already see that Pauli blocking forbids the photo-created pair to form a standard exciton because the

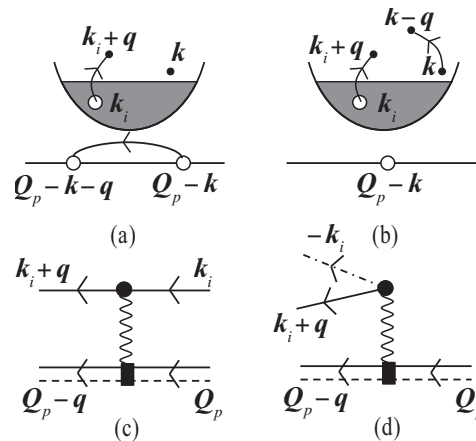


FIG. 3: The valence hole ($Q_p - k$), as in (a), or the conduction electron k , as in (b), can scatter through Coulomb interaction with an electron k_i inside the FS. Processes (a,b) lead to the scattering of a Q_p exciton (solid-dashed double line) into a ($Q_p - q$) state through the excitation of a FS electron k_i to a ($k_i + q$) state, as in (c), or equivalently the creation of a FS electron-hole pair ($k_i + q, -k_i$), as in (d). Dot-dashed line represents FS hole.

$|\mathbf{k}| < k_F$ states are occupied, the low- \mathbf{k} states being actually responsible for most of the exciton binding.

The $|i'\rangle$ state in Eq. (2) is not an eigenstate of the semiconductor Hamiltonian because of the Coulomb interactions V_{ee} between conduction electrons and V_{eh} between conduction electrons and the valence hole. The V_{eh} interaction allows the photo-created electron to fly above the FS, as in Fig. 2(b), or excites a FS electron-hole pair, as in Fig. 3(a). The V_{ee} interaction can also excite a FS electron-hole pair, as in Fig. 3(b). So, these two Coulomb interactions lead to

(i) processes in which the photo-created pair keeps its total momentum Q_p , and the FS stays unchanged, as in Fig. 2(c), its role simply being to Pauli-block low-momentum states from participating in the ladder interactions that make an exciton, in this way weakening its binding;

(ii) processes in which the photo-created pair changes its momentum from Q_p to $(Q_p - q)$, while an electron k_i from the FS is excited to $(k_i + q)$ above the FS (see Fig. 3(c)), which is equivalent to saying that a FS electron-hole pair $(k_i + q, -k_i)$ is created (see Fig. 3(d)).

Including more Coulomb processes would lead to the excitation of more FS electron-hole pairs. These multiple pair excitations eventually change the step-like line shape of the excitation spectra near the onset of band-to-band transitions into a power-law divergence known as Fermi edge singularity, significant for high doping only. For low and intermediate doping regimes as considered here, states that involve zero or one FS electron-hole pair shall provide suitable trial states; then, the Fermi sea not only produces a “truncated” exciton, *i.e.*, an exciton without correlation from low- \mathbf{k} electrons, but also reacts

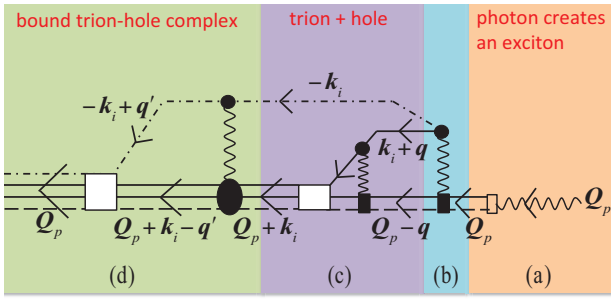


FIG. 4: The Coulomb interaction between the photoexcited exciton \mathbf{Q}_p and a conduction electron \mathbf{k}_i in the FS produces a FS electron-hole pair $(\mathbf{k}_i + \mathbf{q}, -\mathbf{k}_i)$, as in (b). A bound trion can be formed through the repeated scatterings between the exciton and the FS electron flying above the FS, as in (c). When the FS is sizable, the hole $(-\mathbf{k}_i)$ left in the FS can swim inside the FS to form a bound state with the trion, *i.e.*, a bound trion-hole complex, as in (d).

to the excitonic dipole through the excitation of one FS electron-hole pair.

Considering the excitation of just one pair already engages a very interesting new physics. Indeed, with four particles—one valence hole, one FS hole, and two electrons above the FS—complex structures can emerge: the photoexcited exciton can attract a conduction electron from the FS to form a bound trion if the two electrons have opposite spins (see Fig. 4(c)), as a result of repeated ladder-like interactions between the electron and the exciton, as shown in Fig. 3(c). Here also, the FS Pauli blocks low-momentum electron states from participating in the formation of a bound trion. So, compared to exciton, this sets an even stricter upper limit to the doping level for such bound trion to exist. The negatively-charged trion can further attract the FS hole to form a bound trion-hole complex (see Fig. 4(d)). For this attraction to produce a bound state, the hole subspace must be large enough to allow repeated scattering, thus putting an even lower limit to the Fermi-sea size. This leads to a rather narrow window for the trion-hole complex to exist. Note that, the scenario in which the 4-particle system would form a biexciton made of an exciton constructed with a valence hole and an exciton constructed with a FS hole, is not likely to occur because the latter pair does not form an exciton due to the improper hole band structure.

When the Fermi sea increases, more electron states are Pauli-blocked. In addition, this increase produces a stronger screening on the Coulomb interaction. For these two reasons, the bound trion would end by dissociating into an electron and an exciton when the doped Fermi sea gets too large. However, at some stage prior to trion dissociation, the FS hole sets in with the yet-dissociated electron to dress the exciton into a more stable exciton-polaron, while the trion character stays in the excited states of the 4-particle complex. As a result, when the

doping increases, the 4-particle system undergoes a transition from a trion-hole complex to an exciton-polaron. The main purpose of this work is to study when and how such a cross-over takes place, and how the excitation spectrum behaves through the cross-over.

To determine this cross-over, we must derive the ground and low-lying excited states of the 4-particle system made of one valence hole, one FS hole and two electrons above the FS. This is best done through the Rayleigh-Ritz variational procedure. In this procedure, a set of restricted carrier bases is used to find the Hamiltonian eigenstates, the precision of which increases with the number of states included in the basis. Throughout this work, the valence hole mass is taken as infinite—a reasonable approximation since typical semiconductors have a valence hole mass 5 to 10 times larger than the conduction electron mass. This approximation enhances the physical effects associated with the formation of these 4-body complexes without qualitatively changing their physics. Including a finite hole mass is possible but would require far heavier numerical work.

So far, we have omitted the particle spin degrees of freedom. Yet, they are indispensable for the present problem because trion bound states exist only when electrons have opposite spins. In addition, while all particles interact via the same Coulomb interaction regardless of their spins, only same-spin fermions mutually suffer Pauli blocking. So, changing the polarization of the Fermi sea provides an interesting means to study resonance states.

The Hamiltonian for the electron-hole system we here consider reads as

$$H = H_0 + V_{ee} + V_{eh}. \quad (3)$$

For infinitely heavy valence hole, the kinetic part reduces to $H_0 = \sum_{\mathbf{k},s} \varepsilon_{\mathbf{k}} a_{\mathbf{k},s}^\dagger a_{\mathbf{k},s}$, where $a_{\mathbf{k},s}^\dagger$ creates a conduction electron with momentum \mathbf{k} , spin $s = \pm 1/2$ and energy $\varepsilon_{\mathbf{k}} = \hbar^2 \mathbf{k}^2 / 2m_e^*$ with m_e^* being the conduction-electron effective mass. The Coulomb interaction between conduction electrons is given by

$$V_{ee} = \frac{1}{2} \sum_{\mathbf{q} \neq 0} v_{\mathbf{q}} \sum_{\mathbf{k}_1, s_1} \sum_{\mathbf{k}_2, s_2} a_{\mathbf{k}_1 + \mathbf{q}, s_1}^\dagger a_{\mathbf{k}_2 - \mathbf{q}, s_2}^\dagger a_{\mathbf{k}_2, s_2} a_{\mathbf{k}_1, s_1}, \quad (4)$$

while the electron-valence hole part is given by

$$V_{eh} = - \sum_{\mathbf{q} \neq 0} v_{\mathbf{q}} \sum_{\mathbf{k}_1, s_1} \sum_{\mathbf{k}_2, s_2} a_{\mathbf{k}_1 + \mathbf{q}, s_1}^\dagger b_{\mathbf{k}_2 - \mathbf{q}, s_2}^\dagger b_{\mathbf{k}_2, s_2} a_{\mathbf{k}_1, s_1}, \quad (5)$$

where $b_{\mathbf{k},s}^\dagger$ creates a \mathbf{k} valence hole with spin s . The screened Coulomb scattering is taken as

$$v_{\mathbf{q}} = \bar{v}_{\mathbf{q}} / \kappa_{\mathbf{q}}, \quad (6)$$

where

$$\bar{v}_{\mathbf{q}} = \frac{2\pi e^2}{A \varepsilon_{sc} q (1 + qr_0)} \quad (7)$$

is the bare Coulomb potential in undoped 2D (when $r_0 = 0$) or quasi-2D (when r_0 is finite) semiconductors. A is the 2D sample area and ϵ_{sc} is the semiconductor static dielectric constant. The function κ_q accounts for the Thomas-Fermi screening due to doped electrons. Its dependence on the FS electron density, through the Fermi wave vector k_F , is given by $\kappa_q = 1 + s_q/q(1 + qr_0)$ with $s_q = n_p/a_X$ for $q \leq 2k_F$ and $s_q = n_p(1 - \sqrt{1 - (2k_F/q)^2})/a_X$ for $q > 2k_F$, with $n_p = 1$ for fully polarized FS and $n_p = 2$ for unpolarized FS [see Ref. 35]. It has been shown that Eq. (7) can suitably describe the Coulomb interaction in quasi-2D semiconductors such as III-V and II-VI QWs^{3,34}. For an electron interacting with the heavy hole in GaAs/GaAs/Al_xGa_{1-x}As QWs, the parameter r_0 varies from 2nm to 3nm for QWs with well width from 5nm to 8nm and $x = 0.25$. Here we consider the case $r_0 = 0.3a_X$ with $a_X \simeq 10$ nm for GaAs and 3.3nm for ZnSe⁴. The quasi-2D Coulomb potential used here is similar to the expression $\bar{v}_{\mathbf{q}} = 4e^2/A\epsilon_{sc}q \tan^{-1}(qL/q)$ suggested in Ref. 9, where q_L is a parameter depending on the quantum-well width. Note that in real space the quasi-2D Coulomb potential takes the analytic form^{3,34}

$$\bar{v}(r) = \frac{Z(r/r_0)e^2}{\epsilon_{sc}r} \quad (8)$$

with $Z(x) = \frac{\pi x}{2}(\mathbf{H}_0(x) - N_0(x))$, where $\mathbf{H}_0(x)$ and $N_0(x)$ denote the Struve and Neuman functions of zeroth order, respectively. As r_0 goes to zero, $Z(r/r_0)$ goes to 1. As pointed out in Ref. 36, the static screening is a valid approximation when the exciton binding is a small fraction of the band gap, as in III-V and II-VI semiconductor QWs. For 2D materials such as TMDs, the dynamic screening may have to be taken into account. Our main purpose here is to present a detailed study of the exciton-trion-hole cross-over behavior for 2D and quasi-2D systems where static screening is a good approximation. We will not here delve into dynamic screening and band structure effects (including valley degrees of freedom and the spin splitting)²¹ which are important for TMDs.

III. BASIS FOR THE RAYLEIGH-RITZ VARIATIONAL PROCEDURE

For a valence hole mass taken as infinite, the centers of mass of the exciton and the related complexes are fixed on the valence hole. Their energies and wave functions are associated with the relative motions of the light-mass conduction particles located at \mathbf{r}_i from the valence hole. The set of basis functions to represent conduction particles, with 2D polar coordinates $\mathbf{r} = (r, \varphi_r)$, can be taken as

$$\langle \mathbf{r} | \phi_{n,m} \rangle = e^{im\varphi_r} f_{n,m}(r), \quad (9)$$

where $m = (0, \pm 1, \pm 2, \dots)$ labels the angular part and $n = (0, \pm 1, \pm 2, \dots)$ labels the radial part. By noting

that the conduction particles bound to the valence hole have a node at the origin except when $m = 0$, we take the radial part of the basis functions as

$$f_{n,m}(r) = r^{(1-\delta_{m,0})} e^{-\alpha_n r}, \quad (10)$$

the radial extension being controlled by the parameter α_n that we take as $\alpha_0 g^n$. A few (m, n) 's are sufficient to get fast convergence, for α_0 and g properly chosen to cover the physical range of interest. We find that g , which corresponds to the ratio of two consecutive extensions, is better taken between 1.5 and 2; the overlaps between the basis functions are then small enough to avoid numerical instability in the variational calculation. In the present work, we have taken $g = 2$ (1.8) when 8 (10) radial basis functions are used. Choosing a smaller g would lower the ground-state energy slightly (e.g. by $10^{-4}R_X$ where R_X is the 3D exciton ground-state energy), but the numerical computation will suffer larger round-off error when a large number of basis functions are needed. We wish to note that the basis functions are orthogonal with respect to the angular index but *not* with respect to the radial index, that is, $\langle \phi_{n,m} | \phi_{n',m'} \rangle = 0$ for $m \neq m'$ but not for $n \neq n'$.

To study the effect of Pauli blocking by FS electrons in an easy way, we turn from $\langle \mathbf{r} | \phi_{n,m} \rangle$ to $\langle \mathbf{k} | \phi_{n,m} \rangle$. For $\mathbf{k} = (k, \varphi_k)$, this 2D Fourier transform follows from

$$\langle \mathbf{k} | \phi_{n,m} \rangle = \int_A d^2r \langle \mathbf{k} | \mathbf{r} \rangle \langle \mathbf{r} | \phi_{n,m} \rangle \equiv \frac{1}{\sqrt{A}} e^{im\varphi_k} F_{n,m}(k), \quad (11)$$

with $\langle \mathbf{k} | \mathbf{r} \rangle = e^{-i\mathbf{k}\cdot\mathbf{r}}/\sqrt{A}$. For a sample disc with area $A = \pi R^2$, the radial part then reads

$$F_{n,m}(k) = \int_0^R r dr f_{n,m}(r) \int_0^{2\pi} d\varphi e^{-im\varphi} e^{-ikr \cos \varphi}. \quad (12)$$

The integral over $\varphi = \varphi_r - \varphi_k$ gives $(-i)^m 2\pi J_m(kr)$, where $J_m(kr)$ is the Bessel function of order m . As the remaining integrand is bounded by $f_{n,m}(r)$, the r upper boundary can be extended to infinity. Then, the result simply follows from first or second derivative over $(-\alpha_n)$ of the same integral calculated without the $r^{2-\delta_{m,0}}$ factor. This leads to

$$F_{n,m}(k) = 2\pi (-i)^m \left(-\frac{\partial}{\partial \alpha_n} \right)^{2-\delta_{m,0}} \left[\frac{(\sqrt{\alpha_n^2 + k^2} - \alpha_n)^{|m|}}{k^{|m|} \sqrt{\alpha_n^2 + k^2}} \right]. \quad (13)$$

IV. EXCITON WITH A FROZEN FERMI SEA

Let us first consider how the photocreated exciton, made of a conduction electron with spin $(-1/2)$ and a valence hole with angular momentum $(3/2)$ is affected by the occupied electron states in a Fermi sea, $|F_{N_+, N_-}\rangle$, having N_+ electrons with spin $(1/2)$ and N_- electrons with spin $(-1/2)$. In this section, we shall focus on the

effect of Pauli blocking induced by the FS on this exciton. So, for the moment we forget electron-hole pair excitations from the Fermi sea due to Coulomb interaction with the exciton, that is, we take the Fermi sea as frozen.

We obtain the exciton eigenstates i by solving the Schrödinger equation

$$(H - E_i^{(e)})|\Psi_i^{(e)}\rangle = 0. \quad (14)$$

Using the basis functions that we have previously introduced for conduction electrons, we expand exciton states $|\Psi_i^{(e)}\rangle$ with angular momentum m_i

$$|\Psi_i^{(e)}\rangle = \sum_n x_{n,m_i}^{(i)} |n, m_i\rangle \quad (15)$$

on conduction electron-valence hole pair states taken as

$$|n, m\rangle = \sum_{\mathbf{k}} \langle \mathbf{k} | \phi_{n,m} \rangle a_{\mathbf{k}, -\frac{1}{2}}^\dagger b_{\mathbf{Q}'_p, \frac{3}{2}}^\dagger |F_{N_+, N_-}\rangle, \quad (16)$$

where $\mathbf{Q}'_p + \mathbf{k}$ is equal to the absorbed photon momentum \mathbf{Q}_p due to momentum conservation kept by Coulomb processes. Note that Pauli blocking with the Fermi sea imposes $|\mathbf{k}|$ in the above sum to be larger than the Fermi momentum k_{F-} of the N_- electrons.

We project the above $|\Psi_i^{(e)}\rangle$ over $\langle n', m_i |$. The projection over states with $m'_i \neq m_i$ readily gives zero due to the orthogonality of the $|\phi_{n,m}\rangle$ states. This leads to a set of coupled equations for the $x_{n,m_i}^{(i)}$ coefficients,

$$\sum_n \langle n', m_i | H - E_i^{(e)} | n, m_i \rangle x_{n,m_i}^{(i)} = 0, \quad (17)$$

which depend on the number of $|n, m_i\rangle$ basis states taken in the $|\Psi_i^{(e)}\rangle$ expansion. By numerically solving the resulting equation, we can compute the eigenstates and eigenvalues $E_i^{(e)} = \mathcal{E}_i^{(e)} + \mathcal{E}_{N_+, N_-}$ for excitons with angular momentum m_i in the presence of the $|F_{N_+, N_-}\rangle$ Fermi sea having energy \mathcal{E}_{N_+, N_-} . The matrix elements needed to perform this calculation are given in Appendix I.

• **In the absence of Fermi sea**, that is, for $N_+ = N_- = 0$, the 2D exciton energies are analytically known⁴⁰ as $\mathcal{E}_n^{(e)} = -(n - 1/2)^{-2} R_X$ labeled with the principal quantum number n , where R_X is the 3D exciton ground-state energy. The Rayleigh-Ritz variational procedure we here use gives this analytical exciton ground-state energy by just taking *one* radial basis function with $\alpha_0 = 2a_X^{-1}$. By taking 10 radial basis functions with $n = (0, 1, 2, \dots, 9)$ and $\alpha_0 = 0.125a_X^{-1}$, and 5 angular basis functions with $m = (0, \pm 1, \pm 2)$, we also obtain the energies of the $2s$, $2p$, and $3d$ excited states in agreement with the analytical 2D exciton values within an error less than $2 \times 10^{-4} R_X$. For quasi-2D QW, the exciton binding is approximately one half of that in the 2D case, a result consistent with the previous finding³ for GaAs/Al_xGa_{1-x}As QW with width around 10nm and $x = 0.25$.

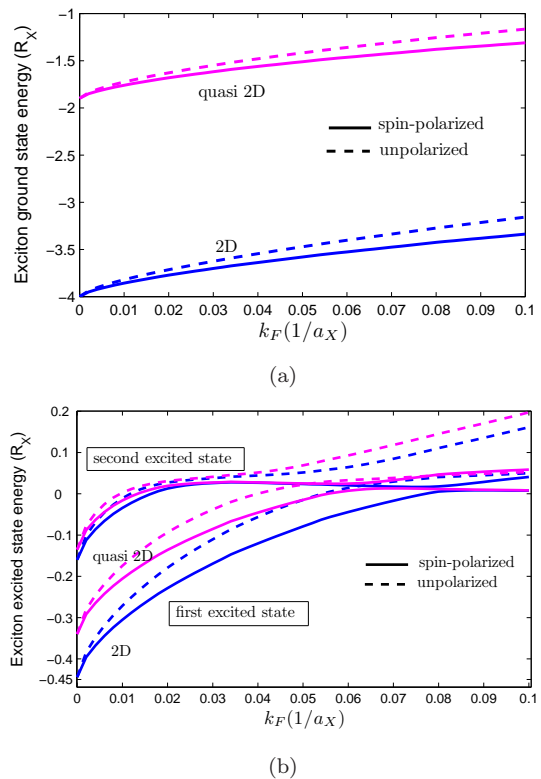


FIG. 5: Energies of the exciton ground state (a) and first two excited states (b) with angular momentum $m = 0$ as functions of k_F for 2D (blue) and quasi-2D (pink) QW. Solid (dashed) curves are for spin-polarized (unpolarized) Fermi sea.

• **In the presence of a fully polarized Fermi sea**, that is, for $N_+ = N$ and $N_- = 0$, the photocreated electron does not feel Pauli blocking from the Fermi sea. Still, a screening effect produced by the conduction electrons goes to weaken the strength of the Coulomb potential, and consequently reduces the binding energies of all bound states. Figure 5 shows a significant reduction of the binding energies of the exciton ground and first two excited states when the doping density increases, as obtained by using the Thomas-Fermi screening in Eq. (6). We find that the first (second) excited state becomes unbound when $k_F a_X$ exceeds 0.078 (0.016) for 2D QW. For quasi-2D QW, they become unbound when $k_F a_X$ exceeds 0.056 and 0.014, respectively. By contrast, the ground states for 2D and quasi-2D remain bound for all values of k_F considered (see the red dash-dotted curves in Fig. 6).

• **In the presence of an unpolarized Fermi sea**, that is, for $N_+ = N_- = N/2$, not only the Coulomb potential is screened, but also the \mathbf{k} sum in Eq. (16) is restricted to $|\mathbf{k}|$ larger than the Fermi momentum k_F . We performed the calculation using basis functions $F_{n,m}(k)$ given in Eq. (13) for $n = (0, 1, 2, \dots, 9)$ with $k > k_F$ and $\alpha_0 = k_F + 0.125a_X^{-1}$. The minimum value of α_n is chosen to be slightly larger than k_F , since any basis function with α smaller than k_F will have too strong overlap with

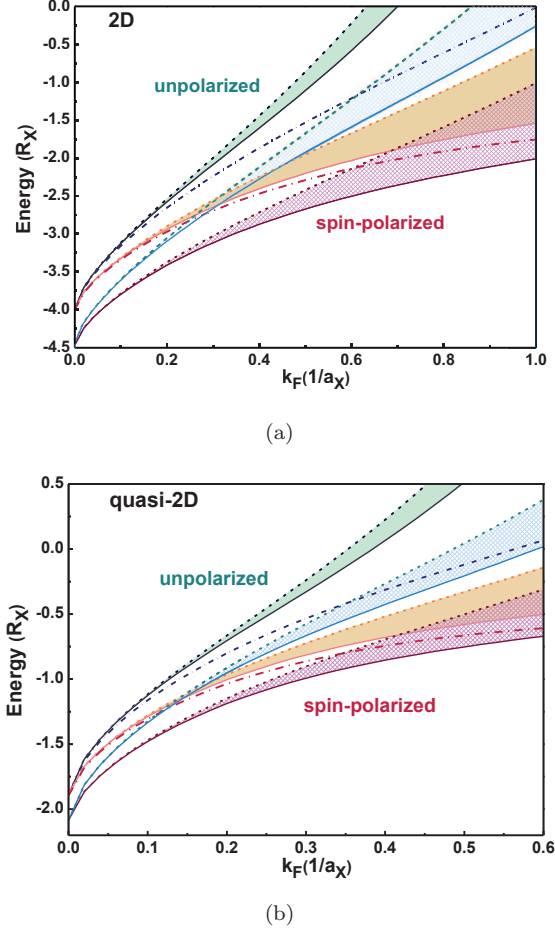


FIG. 6: (a) 2D and (b) quasi-2D QWs. In both cases, the energies of ground-state exciton (red and dark-blue dash-dotted curves), ground-state trion (brown and green dashed curves), trion minus E_F (brown and light-blue solid curves), trion first excited state (orange and black dashed curves), and trion first excited state minus E_F (orange and black solid curves) are shown. The lower (upper) group of curves is for spin-polarized (unpolarized) FS. The shaded areas indicate a continuum energy range of all possible FS-hole states associated with a given trion state when the interaction between the trion and FS hole states is absent. The upper and lower groups of curves correspond to unpolarized and spin-polarized FS, respectively.

the leading basis function due to the cut-off at $k = k_F$. When $k_F = 0$, this basis set coincides with the one we have used in the absence of Fermi sea. The computed energies of the three lowest-lying states as functions of k_F are shown in Fig. 5. The first (second) excited state becomes unbound when $k_F a_X$ exceeds 0.054 (0.012) and 0.04 (0.01) for 2D and quasi-2D QWs, while the ground states remain bound for all values of $k_F a_X$ considered (see the dark-blue dash-dotted curves in Fig. 6).

V. TRION WITH A FROZEN FERMI SEA

We now consider the possibility of forming a trion by the Coulomb interaction between a conduction electron and the excitonic pair created by a σ_+ photon, in the presence of a frozen Fermi sea $|F_{N_+, N_-}\rangle$. By again taking the Fermi sea as frozen, we continue our focus on the effect of Pauli blocking on the 3-particle complex. First, we note that in order to possibly form a bound trion, the two conduction electrons of this complex must have opposite spins. So, the system we consider actually has $(N_+ + 1)$ up-spin electrons and $(N_- + 1)$ down-spin electrons. For $(N_+ = 0, N_- = 0)$, the system reduces to the conventional X^- trion.

To solve the Schrödinger equation

$$(H - E_i^{(ee)})|\Psi_i^{(ee)}\rangle = 0 \quad (18)$$

for this 3-particle complex, we again expand $|\Psi_i^{(ee)}\rangle$ on the basis functions for conduction electrons introduced in Sec. III. By noting that the states possibly seen in photo-absorption have a total angular momentum equal to zero, this expansion can be reduced to

$$|\Psi_i^{(ee)}\rangle = \sum_m \sum_{n_1, n_2} t_{n_1, n_2, m}^{(i)} |n_1, n_2, m\rangle, \quad (19)$$

the 3-particle basis being taken as

$$|n_1, n_2, m\rangle = \sum_{\mathbf{k}_1, \mathbf{k}_2} \phi_{n_1, m}(\mathbf{k}_1) \phi_{n_2, -m}(\mathbf{k}_2) \times a_{\mathbf{k}_1, -\frac{1}{2}}^\dagger a_{\mathbf{k}_2, \frac{1}{2}}^\dagger b_{\mathbf{Q}_p, \frac{3}{2}}^\dagger |F_{N_+, N_-}\rangle, \quad (20)$$

with $\mathbf{Q}'_p + \mathbf{k}_1 + \mathbf{k}_2 = \mathbf{Q}_p + \mathbf{K}$ where \mathbf{K} is the initial momentum of the spin (1/2) electron, due to momentum conservation in Coulomb processes. Note that Pauli blocking forces the above sums over \mathbf{k}_1 and \mathbf{k}_2 to start with values larger than the Fermi momenta of the (N_+, N_-) electrons, respectively.

We use this $|\Psi_i^{(ee)}\rangle$ in the Schrödinger equation (18) for the 3-particle complex and we project it over $\langle n'_1, n'_2, m' |$. This leads to a set of linear equations for the $t_{n_1, n_2, m}^{(i)}$ coefficients

$$\sum_{n_1, n_2, m} \langle n'_1, n'_2, m' | H - E_i^{(ee)} | n_1, n_2, m \rangle t_{n_1, n_2, m}^{(i)} = 0. \quad (21)$$

We numerically solve the above eigenvalue problem to obtain the eigenvalues $E_i^{(ee)} = \mathcal{E}_i^{(ee)} + \mathcal{E}_{N_+, N_-}$. Explicit expressions of the matrix elements needed to perform this calculation are given in Appendix II.

We wish to note that, for infinite valence-hole mass, the prefactors in Eq. (20) do not depend on \mathbf{Q}'_p , or equivalently, on \mathbf{K} ; so, the obtained eigenstates do not depend on the initial momentum of the spin-(1/2) electron added to the photocreated pair. This comment will be of importance in the next section.

• **In the absence of Fermi sea**, the problem reduces to a conventional trion in 2D or quasi-2D systems. The two electrons with spin $(1/2)$ and $(-1/2)$ do not suffer Pauli blocking nor Coulomb screening. For 2D, the computed trion ground-state energy $\mathcal{E}_g^{(ee)}$ is equal to $-4.47R_X$ by taking $(n_1, n_2) = (0, 1, \dots, 7)$, $\alpha_0 = 0.125a_X^{-1}$, and $m = (0, \pm 1, \pm 2)$. This gives a binding energy of trion with respect to exciton equal to $0.47R_X$, in remarkable agreement with the best variational results^{37–39}. When the Fermi sea is present, the same (n, m) 's and α_0 replaced by $k_F + 0.125a_X^{-1}$ show fast convergence for the low-lying states of interest.

• **In the presence of a fully polarized Fermi sea**, that is, for $N_+ = N$ and $N_- = 0$, the photocreated exciton does not suffer Pauli blocking from the FS, but the spin- $(-1/2)$ electron does. The computed trion ground-state energies $\mathcal{E}_g^{(ee)}$ for 2D or quasi-2D systems as functions of k_F are shown by the red dashed curves in Fig. 6.

• **For an unpolarized Fermi sea**, $N_+ = N_- = N/2$, the trion is formed from a linear combination of $(\mathbf{k}_1, \mathbf{k}_2)$ electrons which are both outside their respective Fermi seas. The computed trion ground-state energies for 2D or quasi-2D systems as functions of k_F are shown by the dark-blue dashed curves in Fig. 6.

In the presence of a Fermi sea, we expect that the effects of Pauli blocking and Coulomb screening grow with increasing doping, to ultimately cause the trion to dissociate into an exciton plus a spin- $(-1/2)$ electron sitting on top of the FS (*i.e.* with energy E_F). So, to compare with the exciton ground-state energy in the presence of a Frozen FS as indicated by the dark-blue (red) dash-dotted curve for unpolarized (spin-polarized) FS, we should subtract E_F from the trion ground-state energy, shown as the green (brown) dashed curve in Fig. 6, and the resulting energy is shown as the light-blue (brown) solid curve. For both spin-polarized and unpolarized Fermi seas, the trion remains bound over the entire doping range considered here (with $k_F a_X \leq 1$). As we continue to increase k_F , the trion will dissociate and the trion ground-state energy minus E_F (light-blue and brown solid curves) will merge with the exciton ground-state energy (dark-blue and red dash-dotted curves) in the variational calculation.

To help understand the photo-absorption spectrum of this complex system, we also show in Fig. 6 the energy of the trion first excited state (black and orange dashed curves) and the same energy minus E_F (black and orange solid curves). The trion first excited state merges with the exciton ground state at $k_F = 0$, indicating no bound excited state for the negatively-charged trion in the large valence-hole mass limit. We see that for spin-polarized FS, the trion first-excited-state energy minus E_F (orange solid curve) crosses the trion ground-state energy (brown dashed curve) near $k_F a_X = 0.68$ (0.42) for 2D (quasi-2D) system. No such crossing occurs for unpolarized FS. As will be shown later, this crossing will lead to absorption spectra distinctly different from those for unpolarized FS.

VI. TRION-HOLE COMPLEX

In this section, we consider the possibility that the photocreated exciton can excite one electron out of the Fermi sea, leaving a FS hole (see Fig. 3). This possibility can be included by considering states like

$$a_{\mathbf{k}_2, s}^\dagger a_{\mathbf{k}_1, -\frac{1}{2}}^\dagger b_{\mathbf{Q}'_p, \frac{3}{2}}^\dagger a_{\mathbf{k}_i, s} |F_{N_+, N_-}\rangle, \quad (22)$$

its total momentum $\mathbf{k}_1 + \mathbf{k}_2 + \mathbf{Q}'_p - \mathbf{k}_i$ being equal to the momentum \mathbf{Q}_p of the photocreated exciton and $s = \pm 1/2$. The system we consider now has $N_- + 1$ spin- $(-1/2)$ electrons but N_+ spin- $(1/2)$ electrons only, instead of $N_+ + 1$ as in the previous section. First, we note that the above state must have the (\mathbf{k}_i, s) electron inside the N_s Fermi sea. When $\mathbf{k}_2 = \mathbf{k}_i$, the above state (22) then contains a photocreated electron-hole pair, $a_{\mathbf{k}_1, -1/2}^\dagger b_{\mathbf{Q}'_p, 3/2}^\dagger$, and a full Fermi sea $|F_{N_+, N_-}\rangle$, while for $\mathbf{k}_2 \neq \mathbf{k}_i$, this state has a \mathbf{k}_2 electron above the N_s Fermi sea and a $(-\mathbf{k}_i)$ hole inside. States having more than one FS electron-hole pair are here neglected because we are only interested in low to intermediate doping regime.

We look for the system eigenstates

$$(H - E_i^{(eeh)})|\Psi_i^{(eeh)}\rangle = 0 \quad (23)$$

that have a zero total angular momentum. In general, we can expand the eigenstates of the system in terms of two sets of basis states. The first set contains exciton states (with spin- $(-1/2)$ electron) in the presence of a rigid FS, while the second set contains spin- $(-1/2)$ single electron states accompanied by all possible single electron-hole pair excitations from the FS, $|F_{N_+, N_-}\rangle$. We write

$$|\Psi_i^{(eeh)}\rangle = \sum_j z_{X,j}^{(i)} |\Psi_j^{(e)}\rangle \quad (24)$$

$$+ \sum_{n_1, n_2, \ell, m_1, m_3, s} z_{n_1, n_2, \ell, m_1, m_3, s}^{(i)} |n_1, n_2, \ell, m_1, m_3, s\rangle,$$

where

$$|n_1, n_2, \ell, m_1, m_3, s\rangle = \sum_{\mathbf{k}_1, \mathbf{k}_2, \mathbf{q}} \phi_{n_1, m_1}(\mathbf{k}_1) \phi_{n_2, -m_1 - m_3}(\mathbf{k}_2)$$

$$\times G_{\ell, m_3}(\mathbf{q}) a_{\mathbf{k}_2, s}^\dagger a_{\mathbf{k}_1, -\frac{1}{2}}^\dagger b_{\mathbf{Q}'_p, \frac{3}{2}}^\dagger a_{\mathbf{q}, s} |F_{N_+, N_-}\rangle. \quad (25)$$

In order to identify the trion character contained in the low-lying eigenstates, we transform the basis set with $m_3 = 0$ and $s = 1/2$ into the trion-hole basis set, which contains products of trion eigenstates found in the previous section and FS hole states with zero angular momentum. Namely, we replace the part $\sum_{n_1, n_2, \ell, m_1} z_{n_1, n_2, \ell, m_1, 0, \frac{1}{2}}^{(i)} |n_1, n_2, \ell, m_1, 0, \frac{1}{2}\rangle$ in the above expansion by

$$\sum_j \sum_{|\mathbf{q}| < k_{F_+}} z_{T,j}^{(i)}(\mathbf{q}) a_{\mathbf{q}, \frac{1}{2}} |\Psi_j^{(ee)}\rangle, \quad (26)$$

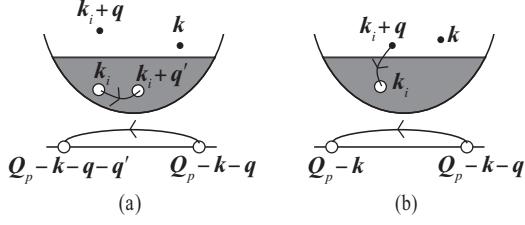


FIG. 7: We start from the configuration of Fig. 3(a), with $(\mathbf{k}, -1/2)$ and $(\mathbf{k}_i + \mathbf{q}, 1/2)$ electrons above the FS, a $(-\mathbf{k}_i, -1/2)$ hole inside the FS, and a $(\mathbf{Q}_p - \mathbf{k} - \mathbf{q}, 3/2)$ valence hole. (a) The FS hole \mathbf{k}_i scatters into a $(\mathbf{k}_i + \mathbf{q})$ state inside the FS through Coulomb interaction with the valence hole. This valence hole can have similar Coulomb interactions with the \mathbf{k} and $(\mathbf{k}_i + \mathbf{q})$ electrons outside the FS (not shown). (b) Through Coulomb interaction with the valence hole, the FS electron-hole pair $(\mathbf{k}_i + \mathbf{q}, -\mathbf{k}_i)$ can also recombine. This leaves a conduction electron-hole pair $(-1/2, 3/2)$ with momentum $(\mathbf{k}, \mathbf{Q}_p - \mathbf{k})$ in the presence of the full Fermi sea, just after the photocreation of a \mathbf{Q}_p exciton.

where

$$z_{T,j}^{(i)}(\mathbf{q}) = \sum_{\ell} z_{T,j,\ell}^{(i)} G_{\ell,0}(\mathbf{q}). \quad (27)$$

The remaining basis states correspond to single electron-hole excitations from the spin- $(1/2)$ FS with $m_3 \neq 0$ or from the spin- $(-1/2)$ FS with all possible m_3 , if $N_- \neq 0$.

In the above equation, a finite set of basis functions $G_{\ell,m_3}(\mathbf{q})$ is further needed to describe Coulomb scatterings between the FS hole \mathbf{q} in the Fermi sea and the three particles of the trion [See Fig. 7(a)]. $G_{\ell,m}(\mathbf{q})$ is taken as a set of orthogonal basis functions

$$G_{\ell,m}(\mathbf{q}) = (-i)^m e^{im\varphi_{\mathbf{q}}} \sqrt{\frac{2\pi(2 - \delta_{\ell,0})}{k_F q}} \cos \frac{\ell\pi q}{k_F}. \quad (28)$$

These scatterings ultimately lead to a trion-hole complex. The trion-hole states are coupled to the exciton states $|\Psi_j^{(e)}\rangle$ in Eq. (24) in the eigenstates of the 4-particle complex by the Coulomb interaction, as shown in Fig. 7(b).

Since both the system eigenstates $|\Psi_i^{(eeh)}\rangle$ and the trion states $|\Psi_j^{(ee)}\rangle$ in Eq. (24) have zero total angular momentum, the trion-hole envelope function $z_{T,j}^{(i)}(\mathbf{q})$ must be s -like. The angular correlations between trion and FS hole with $m_3 \neq 0$ are included in the remaining terms of Eq. (24). We also wish to note that the scattering between trion and FS hole induces a change to the trion momentum. However, when the valence hole mass is infinite, the trion states no longer depend on their center-of-mass momentum. This is why we can use the previously obtained trion states in Eq. (26).

We now project the Schrödinger equation (23) onto the exciton states $|\Psi_j^{(e)}\rangle$, the trion-hole states $a_{\mathbf{q},\frac{1}{2}}|\Psi_j^{(ee)}\rangle$, and the remaining basis states of the form $|n_1, n_2, \ell, m_1, m_3, s\rangle$. This leads to a set of coupled

equations, from which we determine the $z_{n_1, n_2, \ell, m_1, m_3, s}^{(i)}$ coefficients that enter $|\Psi_i^{(eeh)}\rangle$. In numerically solving Eq. (23), we have used 8 basis states with $n = (0, 1, \dots, 7)$ and $m = 0$ for $|\Psi_j^{(e)}\rangle$, twenty $G_{\ell,0}(\mathbf{q})$ functions with $\ell = (0, 1, \dots, 19)$, multiplied by the lowest 64 trion eigenstates obtained from solving Eq. (18) in the basis defined in Eq. (20). Also included are the basis states $|n_1, n_2, \ell, m_1, m_3, s\rangle$ with $(n_1, n_2) = (0, 1, \dots, 7)$, $\ell = (0, 1, \dots, 9)$, and $(m_1, m_2, m_3) = (0, \pm 1, \pm 2)$, while keeping $m_1 + m_2 + m_3 = 0$. For spin-polarized FS with $N_- = 0$, only the additional basis states with $s = 1/2$ and $m_3 = (1, 2)$ are included, while for unpolarized FS, we need to include basis states with $s = -1/2$ and $m_3 = (0, 1, 2)$.

The $|\Psi_i^{(eeh)}\rangle$ state is trion-hole like when the squared amplitude $f_T^{(i)} = \sum_{|\mathbf{q}| < k_F} |z_{T,g}^{(i)}(\mathbf{q})|^2$ containing the ground-state trion component is close to 1: The trion character then dominates. Here i labels the eigenstates of the 4-particle complex. In the other limit, $f_X^{(i)} = |z_{X,g}^{(i)}|^2$ containing the ground-state exciton component is much larger than $f_T^{(i)}$, and the $|\Psi_i^{(eeh)}\rangle$ state is better seen as exciton-polaron like, that is, an exciton dressed by FS electron-hole pairs.

Figure 8 shows the ground-state energy of the 4-particle complex as a function of k_F as the orange (dark-blue) thick solid curve for spin-polarized (unpolarized) FS. The red (green) dashed curve represents the trion ground state plus a hole at the bottom of the spin-polarized (unpolarized) FS, while the purple (green) thin solid curve represents the trion ground state plus a hole at the top of the FS, when the interaction between trion and FS hole is absent. So, the energy for the thin solid curve is equal to the trion ground-state energy minus the Fermi energy, $E_F = \hbar^2 k_F^2 / (2m_e^*)$. Between the dashed and thin solid curves is a continuum of states (indicated by shaded areas) that consist of the trion ground state and a FS hole having energy between 0 and $-E_F$. When the interaction between trion and FS hole is taken into account, the energy of the 4-particle complex ground state lowers to the thick solid curve. The fact that this curve is well separated from the continuum shows that the 4-particle complex forms a bound state. We note that for both spin-polarized and unpolarized Fermi seas, the dashed curve crosses the dash-dotted curve (which indicates the energy of the exciton ground state with a Frozen FS) at $k_F a_X \simeq 0.6$ for 2D QW and at $k_F a_X \simeq 0.34$ for quasi-2D QW. Beyond the crossing point, the exciton ground-state level merges into the continuum of trion-hole states (shaded areas) and the two different species become strongly coupled. This also signals the advent of the cross-over from trion-hole complex to exciton-polaron.

As discussed in the introduction, the character of this 4-particle ground state as a function of k_F can be revealed by the squared amplitude of the trion component, $f_T^{(0)}$ and the squared amplitude $f_X^{(0)}$ of the exciton compo-

ment shown in Fig. 1, with a cross-over for spin-polarized (unpolarized) FS occurring at $k_F a_X = 0.81$ (0.72) for 2D and at 0.45 (0.4) for quasi-2D. For doping densities above the cross-over, the ground state of the 4-particle complex maintains a strong exciton component, as evidenced by its squared amplitude shown in Fig. 1. The fact that this energy is lower than the exciton state by $\approx 0.7R_X$ ($0.25R_X$) for 2D (quasi-2D) indicates a binding of the exciton with a pair of FS electron and hole, which can be seen as exciton-polaron in the weak polaron limit. The sum of $f_T^{(0)}$ and $f_X^{(0)}$ is very close to 1 at low doping but becomes less than 1 at high doping; the deviation from 1 is attributed to the fraction contributed by the exciton excited states with amplitude $z_{X,j \neq g}^{(0)}$ and the trion excited states with amplitude $z_{T,j \neq g}^{(0)}$ (\mathbf{q}) in the 4-particle ground state. Obviously, these contributions become more significant as the doping increases. It is interesting to note that for spin-polarized (unpolarized) FS, the binding energy of the 4-particle complex with respect to the exciton plus a frozen FS increases steadily from $0.47R_X$ to $0.60R_X$ ($0.58R_X$) as $k_F a_X$ increases from 0 to 0.7 for 2D QW, and from $0.19R_X$ to $0.22R_X$ ($0.20R_X$) as $k_F a_X$ increases from 0 to 0.5 for quasi-2D QW. This feature can be attributed to the increase in correlation energy as the FS hole gains more available states within the FS when k_F increases. This energy gain then overcomes the reduction of the trion binding energy caused by Pauli blocking. When many FS electron-hole pairs are included, the nature of this state will totally change. However, this regime as expected for high doping is beyond the scope of this paper.

The cross-over from trion-hole complex to exciton-polaron can be seen from photo-absorption experiments. The final state $|f\rangle$ in Eq. (1) then is the $|\Psi_i^{(eeh)}\rangle$ state of Eq. (24). The photo-absorption spectrum associated with the trion-hole complex or the exciton-polaron follows from

$$\begin{aligned} A(\omega) &\propto \sum_i |\langle \Psi_i^{(eeh)} | \sum_{\mathbf{k}} a_{\mathbf{k}, -\frac{1}{2}}^\dagger b_{-\mathbf{k}+\mathbf{Q}_p, \frac{3}{2}}^\dagger | F_{N_+, N_-} \rangle|^2 \\ &\quad \times |\hat{\mathbf{e}}_p \cdot \mathbf{P}_{cv}|^2 \delta(\hbar\omega - E_g - \mathcal{E}_i^{(eeh)}) \quad (29) \\ &\approx \sum_i \frac{|\hat{\mathbf{e}}_p \cdot \mathbf{P}_{cv}|^2 |\sum_{n,j} z_{X,j}^{(i)} x_{n,0}^{(j)} C_{n,0} \tilde{f}_{n,0}(0)|^2}{(\hbar\omega - E_g - \mathcal{E}_i^{(eeh)})^2 + \gamma^2}, \end{aligned}$$

where $\tilde{f}_{n,0}(r)$ is the radial part of the $m=0$ exciton basis state defined in Eq. (A.28) with $\tilde{f}_{n,0}(0) = 1$ for polarized FS and $\tilde{f}_{n,0}(0) = 1 - \int_0^{k_F} k dk I_0(\alpha_n, k) = \alpha_n / \sqrt{\alpha_n^2 + k_F^2}$ for unpolarized FS. E_g is the semiconductor band gap, $\hat{\mathbf{e}}_p$ is the photon polarization vector, and $C_{n,0}$ is the normalization factor of the exciton basis state $|n, 0\rangle$ as defined in Eq. (A.7). \mathbf{P}_{cv} is the matrix element of the momentum operator between the valence and conduction band Bloch states, which is essentially \mathbf{k} -independent for the range of \mathbf{k} considered in the present calculation. $z_{X,j}^{(i)}$ is the prefactor of the j exciton in the $|\Psi_i^{(eeh)}\rangle$ state given in Eq. (24), and $x_{n,0}^{(j)}$ is the prefactor of the $|n, 0\rangle$ basis

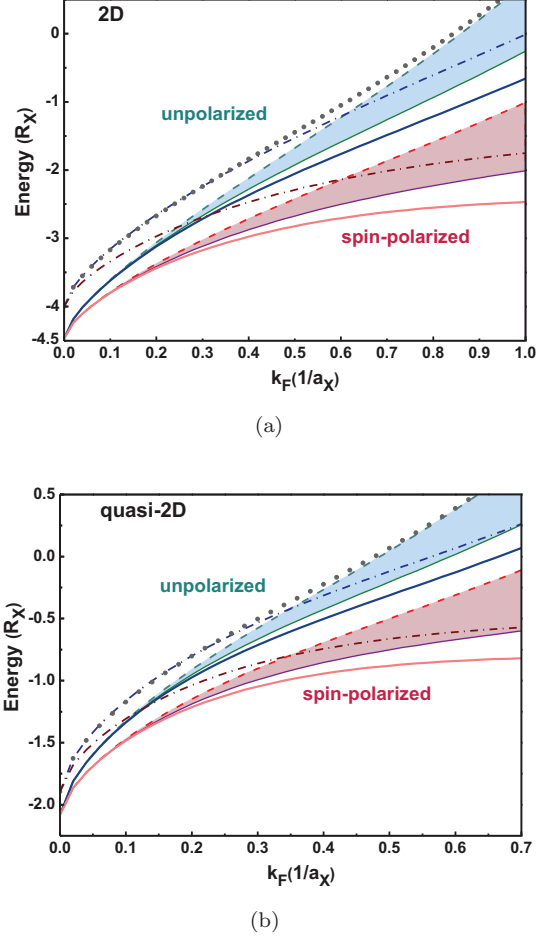


FIG. 8: (a) 2D (b) quasi-2D QW. In both cases, the energies of ground-state exciton (brown and blue dash-dotted curves), ground-state trion (red and green dashed curves), and trion-hole complex evolving to exciton-polaron (orange and dark-blue thick solid curves) are shown. The lower (upper) group of curves is for spin-polarized (unpolarized) Fermi sea. The shaded area indicates a continuum energy range of all possible trion-hole states when the interaction between the trion and FS hole states is absent. The solid spheres delineate the energy positions of the upper branch of the coupled mode between trion-hole complex and exciton-polaron for unpolarized FS, which correspond to the second peak in the absorption spectra in Figs. 9(a) and Fig. 10(a)

state in the exciton state j given in Eq. (15). Results are presented with the $\delta(x)$ peak replaced by $1/(x^2 + \gamma^2)$ where γ is a phenomenological absorption-line broadening taken to be equal to $0.015R_X$.

The calculated absorption spectra of doped semiconductors, as a function of k_F (in units of a_X^{-1}), are shown in Figs. 9 and 10 for 2D and quasi-2D, respectively. For clarity, the spectra for different Fermi momenta k_F are vertically shifted by 0.2. For $k_F = 0$, only the exciton ground state peak appears, as the first excited state oc-

curs at $-(4/9)R_X$ ($-0.34R_X$) for 2D (quasi-2D), which is beyond the energy range of interest. As k_F increases, another peak appears at the ground-state energy of the 4-particle complex, whose strength increases as k_F increases, while the strength of the higher-energy peak gradually reduces. Note that the oscillator strength of each absorption peak is directly related to the amount of admixture of the exciton component in that state, since only the exciton is coupled directly to photon.

At low doping, the 4-particle ground state corresponds to a trion weakly dressed by a conduction FS hole, and it turns into an exciton dressed by a FS electron-hole pair as the doping density passes the crossing point, as evidenced by the increasing of oscillator strength. The cross-over occurs for spin-polarized (unpolarized) Fermi sea at $k_F a_X \simeq 0.81$ (0.72) in 2D QW and at $k_F a_X \simeq 0.45$ (0.39) in quasi-2D QW. At the crossing point, the two peaks have nearly the same strength (see Figs. 9 (Fig. 10)). Before the crossing point, the second peak remains exciton-like, sitting at approximately $0.5R_X$ ($0.2R_X$) above the 4-particle ground state for 2D (quasi-2D) QW.

Beyond this crossing point, the exciton state enters the continuum band of the trion-hole excited states as indicated by the shaded area in Fig. 8. The coupling of the exciton with the group of trion-hole states leads to an anti-crossing behavior in much the same manner as in an exciton-polariton, with the “lower branch” being exciton like and the upper branch being trion-hole like. The tracing of the energy of the upper branch of the “coupled mode” is illustrated by solid spheres for unpolarized FS in Fig. 8. It shows that the energy separation between the two main peaks grows wider as k_F continues to increase beyond the crossing point.

For spin-polarized FS, there is an overlap of the trion-hole band associated with the trion ground state (lowest shaded area of Fig. 6) with the trion-hole band associated with the trion first excited state (next shaded area in Fig. 6) when the energy difference between the trion first-excited state and ground state becomes smaller than the band width (E_F) at high enough k_F values. Such overlap produces some extra peaks in the absorption spectrum, as seen in Figs. 9(b) and 10(b) for spin-polarized FS, since both groups of states can pick up some oscillator strength via coupling to the exciton state when their energies are close. The interplay of the two trion-hole bands coupling simultaneously to the exciton state after the cross-over point produces a rich anti-crossing pattern.

To compare our theoretical predictions with experimental observations for II-VI semiconductors, we focus on the quasi-2D QW with unpolarized FS (see Fig. 10(a)). We compare our results with the reflectivity measurements of ZnSe/Zn_{0.89}Mg_{0.11}S_{0.18}Se_{0.82} QW of 8nm well width reported in Ref. 9. Here, we take $R_X = 22\text{meV}$ and $a_X = 3.3\text{nm}$, which correspond to the exciton binding energy and the effective Bohr radius in 3D ZnSe. For the quasi-2D Coulomb potential used here, we obtain an exciton binding energy of $1.896R_X = 42\text{meV}$ and a trion binding energy of $0.188R_X = 4.1\text{meV}$

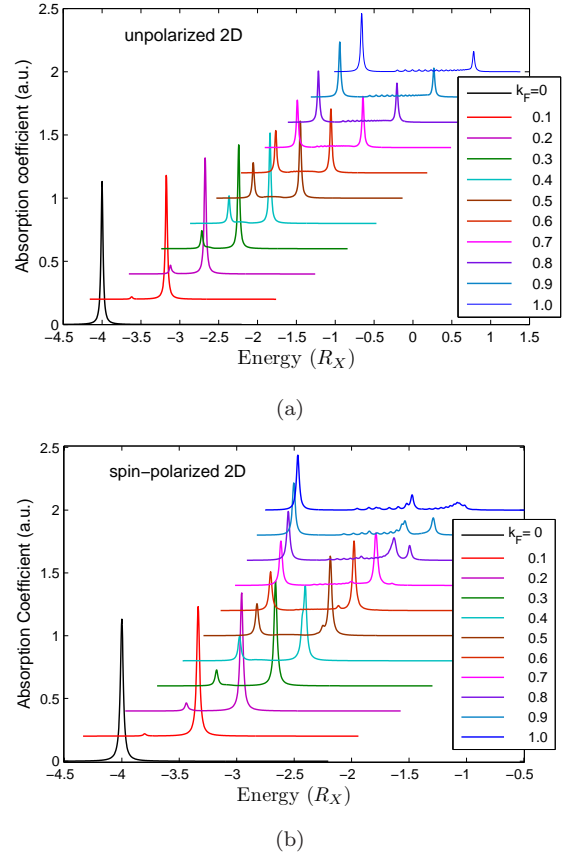


FIG. 9: Absorption spectra of a photo-created electron-hole pair in the presence of (a) an unpolarized FS and (b) a spin-polarized FS for various k_F values (in units of a_X^{-1}), taking into account all possible excitations of single FS electron-hole pair for 2D QW. For clarity, the base lines of spectra with increasing k_F values are vertically shifted up by 0.2 from the pervious curve.

when $E_F = 0$, in good agreement with the experimental values reported in Ref. 9. As E_F increases to 1.7meV , which corresponds to a value of $k_F a_X \approx 0.3$, the observed energy splitting Δ_{XT} between the ground-state peak (trion like) and the excited-state peak (exciton like) increases to 6meV (see Fig. 4(a) of Ref. 9), while our predicted value for this energy difference increases from $0.188R_X = 4.1\text{meV}$ at $E_F = 0$ to $0.209R_X = 4.6\text{meV}$ at $E_F = 1.7\text{meV}$. So, our model calculation predicts the increase of the Δ_{XT} splitting with doping but underestimates the amount of increase observed experimentally. However, as $k_F a_X$ increases to 0.4 (near cross-over point), our predicted value for Δ_{XT} quickly goes up to $0.278R_X = 6.1\text{meV}$. Our model considers only basis states with angular functions up to $m = 2$. By adding more basis functions, we expect the Δ_{XT} splitting to be further increased, in closer agreement with experiment. Furthermore, the electron-to-hole mass ratio considered here is zero. A larger electron-to-hole mass ratio would also increase the electron-hole correlation.

Overall, our results agree qualitatively with experi-

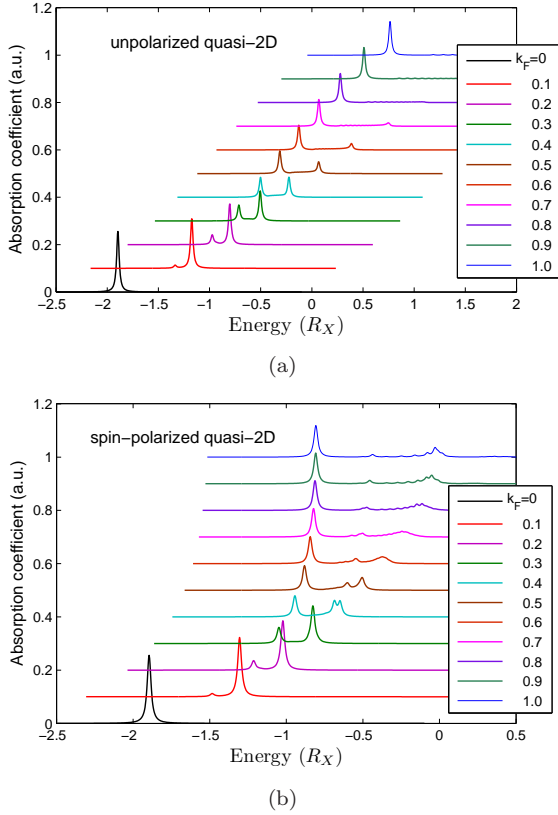


FIG. 10: Same as Fig. 9, but for quasi-2D QW. For clarity, the base lines of spectra with increasing k_F values are vertically shifted up by 0.1 from the pervious curve.

mental observations for many II-VI semiconductor QWs and 2D materials. The energy splitting of the first two absorption peaks (labeled as Δ_{XT}) increases as the doping density increases. It should be stressed that the so-called Δ_{XT} splitting represents the energy difference between the exciton peak and trion state only at $k_F = 0$. For finite k_F , such a splitting represents the energy difference in the two coupled modes of the exciton-polaron and the trion-hole complex. Furthermore, the cross-over behavior predicted here implies that the oscillator strength of the ground-state peak would increase as it picks more admixture of the exciton state, while the excited-state peak would decrease as the doping density increases.

This behavior has been observed experimentally and also predicted theoretically by many-body Green's function approach as reported in Ref. 9.

VII. CONCLUSION

In this work, we study the absorption of a circularly-polarized (σ_+) photon in the presence of an unpolarized or fully polarized Fermi sea made of electrons having a spin different from the photoexcited electron. We only consider single-pair excitations from the FS as induced by Coulomb interaction with the photoexcited exciton, that is, a 4-particle system. We show that at low doping, its ground state essentially corresponds to a trion weakly bound to a FS hole. When the doping increases, the ground state turns into an exciton-polaron because of the increasing effect of Pauli blocking on the trion-hole complex. The cross-over from trion-hole to exciton-polaron occurs for unpolarized (spin-polarized) FS at $k_F a_X = 0.7$ (0.8) for 2D QW, and at $k_F a_X = 0.4$ (0.45) for quasi-2D QW. For a photon with circularly-polarized polarization the photo-absorption spectra show two prominent low-energy peaks that correspond to the coupled states of the trion-hole complex and the exciton-polaron. Their line shapes will be further modified by including more electron-hole pairs in the FS, which will be important in high doping regime. By contrast, if the absorbed photon has a σ_- polarization, the photoexcited electron has spin (1/2). As trion cannot be formed with a polarized FS made of spin-(1/2) electrons, we then have a pure exciton absorption spectrum, the FS possibly leading to Fermi edge singularity. As a result, when using an unpolarized light source, we must see, in addition to the above two peaks associated with exciton-trion-hole coupled states, a higher-energy peak that corresponds to the pure exciton state.

Acknowledgments

This work was supported under Contract No. MOST 107-2112-M-001-032. S.Y. S. would like to thank INSP, CNRS for invitations.

Appendix I. RELEVANT MATRIX ELEMENTS FOR EXCITON STATES

(1) **In the absence of Fermi sea**, the overlap between the conduction electron-valence hole pair states $|n, m\rangle$ defined in Eq. (16) reads as

$$\langle n', m | n, m \rangle = O_{n',n}^{(m)} = C_{n',m} C_{n,m} 2\pi \frac{(3 - 2\delta_{m,0})!}{(\alpha_n + \alpha_{n'})^{4 - 2\delta_{m,0}}} \quad (\text{A.1})$$

with $C_{n',m} = (2\alpha_n)^{2-\delta_{m,0}}/\sqrt{2\pi(3-2\delta_{m,0})}$. The kinetic energy part of the Hamiltonian is given by

$$\begin{aligned}\langle n', m | H_0 | n, m \rangle &= K_{n',n}^{(m)} = 2\pi C_{n',m} C_{n,m} \int_0^\infty dr r^{2-\delta_{m,0}} e^{-\alpha_{n'} r} \frac{1}{2m_e^*} \left(\frac{m^2}{r^2} - \frac{\partial}{r\partial r} \left(r \frac{\partial}{\partial r} \right) \right) r^{1-\delta_{m,0}} e^{-\alpha_n r} \\ &= 2\pi C_{n',m} C_{n,m} \frac{1}{2m_e^*} \left(\frac{m^2 - (1-\delta_{m,0})^2}{(\alpha_n + \alpha_{n'})^{2-2\delta_{m,0}}} + \frac{\alpha_n \alpha_{n'} (3-2\delta_{m,0})!}{(\alpha_n + \alpha_{n'})^{4-2\delta_{m,0}}} \right),\end{aligned}\quad (\text{A.2})$$

while the electron-hole Coulomb part is given by

$$\begin{aligned}\langle n', m | V_{eh} | n, m \rangle &= -2\pi C_{n',m} C_{n,m} \int d\mathbf{r} r^{3-2\delta_{m,0}} e^{-(\alpha_n + \alpha_{n'})r} v(\mathbf{r}) \\ &= -C_{n',m} C_{n,m} \frac{2\pi e^2}{\epsilon_{sc}} \frac{2 - \delta_{m,0}}{(\alpha_n + \alpha_{n'})^{3-2\delta_{m,0}}}.\end{aligned}\quad (\text{A.3})$$

(2) In the presence of a Fermi sea having a Fermi wave vector k_F , wave functions in momentum space, as the basis functions defined in Eq. (13), are more convenient to take into account Pauli blocking. Let us write them as $F_{n,m}(k) = 2\pi(-i)^m I_{1-\delta_{m,0}}^{(m)}(\alpha_n, k)$, with

$$I_L^{(m)}(\alpha, k) = \left(-\frac{\partial}{\partial \alpha} \right)^{L+1} \left[\frac{(f(\alpha) - \alpha)^{|m|}}{k^{|m|} f(\alpha)} \right], \quad (\text{A.4})$$

where $f(\alpha) = \sqrt{\alpha^2 + k^2}$.

For $m = 0$, we have $I_0^{(0)}(\alpha, k) = \alpha/f^3$ and $I_2^{(0)}(\alpha, k) = \alpha(15\alpha^2 - 9f^2)/f^7$, while for $m > 0$,

$$I_1^{(m)}(\alpha, k) = (f - \alpha)^m [(m + 3f')(mf + \alpha) - m\alpha - f]/(k^m f^4) \quad (\text{A.5})$$

and

$$\begin{aligned}I_2^{(m)}(\alpha, k) &= (f - \alpha)^{(m-1)} [4(f - \alpha)f' - m(\alpha - f)] [(m + 3f')(mf + \alpha) - m\alpha - f]/(k^m f^5) \\ &\quad - (f - \alpha)^m [(m + 3f')(mf' + 1) + 3(1/f - \alpha f'/f^2)(mf + \alpha) - m - f']/(k^m f^4),\end{aligned}\quad (\text{A.6})$$

where $f' = \alpha/f$.

The overlap then reads as

$$O_{n',n}^{(m)} = C_{n',m} C_{n,m} \frac{1}{2\pi} \int_{k_F}^\infty k dk F_{n',m}^*(k) F_{n,m}(k), \quad (\text{A.7})$$

with

$$C_{n,m} = 1/\sqrt{\frac{1}{2\pi} \int_{k_F}^\infty k dk |F_{n,m}(k)|^2}. \quad (\text{A.8})$$

We have

$$O_{n',n}^{(0)} = C_{n',0} C_{n,0} \pi \alpha_{n'} \alpha_n J_{n',n}^{(0)}, \quad (\text{A.9})$$

$$O_{n',n}^{(1)} = C_{n',1} C_{n,1} 9\pi \alpha_{n'} \alpha_n M_{n',n}^{(1)}, \quad (\text{A.10})$$

$$O_{n',n}^{(2)} = C_{n',2} C_{n,2} 9\pi \alpha_{n'} \alpha_n M_{n',n}^{(2)}, \quad (\text{A.11})$$

while the kinetic energy part of $\langle n', m | H | n, m \rangle$ reads as

$$K_{n',n}^{(m)} = C_{n',m} C_{n,m} \frac{1}{2\pi} \int_{k_F}^\infty k^3 dk F_{n',m}^*(k) F_{n,m}(k), \quad (\text{A.12})$$

with

$$K_{n',n}^{(0)} = C_{n',0} C_{n,0} \pi \alpha_{n'} \alpha_n J_{n',n}^{(1)}, \quad (\text{A.13})$$

$$K_{n',n}^{(1)} = C_{n',1}C_{n,1}9\pi\alpha_{n'}\alpha_n M_{n',n}^{(2)}, \quad (\text{A.14})$$

$$K_{n',n}^{(2)} = C_{n',2}C_{n,2}9\pi\alpha_{n'}\alpha_n M_{n',n}^{(3)}, \quad (\text{A.15})$$

where

$$J_{n',n}^{(m)} = \int_{k_F^2}^{\infty} du \frac{u^m}{\sqrt{(a+bu+u^2)^3}}, \quad (\text{A.16})$$

$$M_{n',n}^{(m)} = \int_{k_F^2}^{\infty} du \frac{u^m}{\sqrt{(a+bu+u^2)^5}}, \quad (\text{A.17})$$

with $a = (\alpha_{n'}\alpha_n)^2$ and $b = \alpha_{n'}^2 + \alpha_n^2$. Explicit expressions of $J_{n',n}^{(m)}$ and $M_{n',n}^{(m)}$ for the first few m 's are

$$J_{n',n}^{(0)} = -\frac{4}{\Delta} + \frac{2(2k_F^2+b)}{\Delta\sqrt{a+bk_F^2+k_F^4}} \rightarrow \frac{2}{\alpha_{n'}\alpha_n(\alpha_{n'}+\alpha_n)^2} \text{ as } k_F \rightarrow 0, \quad (\text{A.18})$$

$$J_{n,n}^{(0)} = \frac{1}{2(\alpha_n^2+k_F^2)^2}, \quad (\text{A.19})$$

$$J_{n',n}^{(1)} = \frac{2b}{\Delta} + \frac{2(2a+bk_F^2)}{\Delta\sqrt{a+bk_F^2+k_F^4}} \rightarrow \frac{2}{(\alpha_{n'}+\alpha_n)^2} \text{ as } k_F \rightarrow 0, \quad (\text{A.20})$$

$$J_{n,n}^{(1)} = \frac{(\alpha_n^2/2+k_F^2)}{(\alpha_n^2+k_F^2)^2}. \quad (\text{A.21})$$

$$M_{n',n}^{(0)} = \frac{2(2k_F^2+b)}{3\Delta\sqrt{(a+bk_F^2+k_F^4)^3}} - \frac{16}{3\Delta}\left(\frac{2k_F^2+b}{\Delta\sqrt{a+bk_F^2+k_F^4}} - \frac{2}{\Delta}\right) \rightarrow \frac{2}{\alpha_{n'}\alpha_n(\alpha_{n'}+\alpha_n)^2} \text{ as } k_F \rightarrow 0, \quad (\text{A.22})$$

$$M_{n,n}^{(0)} = \frac{1}{4(\alpha_n^2+k_F^2)^4}, \quad (\text{A.23})$$

$$M_{n',n}^{(1)} = \frac{1}{3\sqrt{(a+bk_F^2+k_F^4)^3}} - \frac{b}{2}M_{n',n}^{(0)} \rightarrow \frac{4}{3\alpha_{n'}\alpha_n(\alpha_{n'}+\alpha_n)^4} \text{ as } k_F \rightarrow 0, \quad (\text{A.24})$$

$$M_{n',n}^{(2)} = \frac{k_F^2}{2\sqrt{(a+bk_F^2+k_F^4)^3}} - \frac{b}{4}M_{n',n}^{(1)} + \frac{a}{2}M_{n',n}^{(0)} \rightarrow \frac{4}{3\alpha_{n'}\alpha_n(\alpha_{n'}+\alpha_n)^4} \text{ as } k_F \rightarrow 0, \quad (\text{A.25})$$

$$M_{n',n}^{(3)} = \frac{k_F^4}{\sqrt{(a+bk_F^2+k_F^4)^3}} + 2aM_{n',n}^{(1)} + \frac{b}{2}M_{n',n}^{(2)} \rightarrow \frac{2(b+4\alpha_{n'}\alpha_n)}{3\alpha_{n'}\alpha_n(\alpha_{n'}+\alpha_n)^4} \text{ as } k_F \rightarrow 0. \quad (\text{A.26})$$

with $\Delta = b^2 - 4a = (\alpha_{n'}^2 - \alpha_n^2)^2$.

The matrix elements for the electron-hole Coulomb potential read

$$\langle n', m | \tilde{V}_{eh} | n, m \rangle = -C_{n',m}C_{n,m} \int d\mathbf{r} \tilde{f}_{n',m}(r) \tilde{f}_{n,m}(r) \tilde{V}^{sc}(r), \quad (\text{A.27})$$

where

$$\tilde{f}_{n,m}(r) = f_{n,m}(r) - \int_0^{k_F} k dk J_m(kr) I_{1-\delta_{m,0}}^{(m)}(\alpha_n, k) \quad (\text{A.28})$$

is the radial part of the FS-blocked basis function in real space, and

$$\tilde{V}^{sc}(r) = \frac{e^2}{\epsilon_{sc}} \left[\frac{Z(r/r_0)}{r} - \frac{2\pi}{A} \sum_{\mathbf{q}} \frac{s_{\mathbf{q}}}{q(1+qr_0)(q(1+qr_0)+s_{\mathbf{q}})} e^{i\mathbf{q}\cdot\mathbf{r}} \right], \quad (\text{A.29})$$

where the first term on the right-hand side (RHS) is the bare Coulomb potential and the second term is the screening part which can be evaluated accurately, since the integrand decays quickly with q .

Appendix II. MATRIX ELEMENTS FOR THE ELECTRON-ELECTRON COULOMB POTENTIAL

Since we have excluded the Coulomb interactions with the remaining N electrons, the semiconductor Hamiltonian H is reduced to $H_T + \mathcal{E}_N$, where H_T denotes the Hamiltonian of the three particles (h, e_1, e_2). For infinite valence hole mass, we have

$$H_T = H_1 + H_2 + V_{e_1 e_2}, \quad (\text{B.1})$$

with $H_j = \varepsilon_{\mathbf{k}}^{(e_j)} - V_{e_j h}$. As H_1 does not involve the e_2 electron, its matrix element $\langle n'_1, n'_2, m' | H_1 | n_1, n_2, m \rangle$ reads as $\delta_{m', m} \delta_{n'_2, n_2} \langle n'_1, m | H_1 | n_1, m \rangle$; similarly for $\langle n'_1, n'_2, m' | H_2 | n_1, n_2, m \rangle$. These two matrix elements are orthogonal with respect to angular momentum m . On the other hand, the matrix element for $V_{e_1 e_2}$ is given by

$$\begin{aligned} \langle n'_1, n'_2, m' | V_{e_1 e_2} | n_1, n_2, m \rangle &= C_{n'_1, m'} C_{n'_2, m'} C_{n_1, m} C_{n_2, m} \\ &\times \int d\mathbf{r}_1 \phi_{n'_1, m'}^*(\mathbf{r}_1) \phi_{n_1, m}(\mathbf{r}_1) \int d\mathbf{r}_2 \phi_{n'_2, -m'}^*(\mathbf{r}_2) \phi_{n_2, -m}(\mathbf{r}_2) \tilde{V}^{sc}(|\mathbf{r}_1 - \mathbf{r}_2|) \end{aligned} \quad (\text{B.2})$$

where $\tilde{V}^{sc}(r)$ is given in Eq. (A.29). We end up with

$$\begin{aligned} \langle n'_1, n'_2, m' | V_{e_1 e_2} | n_1, n_2, m \rangle &= C_{n'_1, m'} C_{n'_2, m'} C_{n_1, m} C_{n_2, m} \\ &\times 4\pi^2 \int r_1 dr_1 \tilde{f}_{n'_1, m'}(r_1) \tilde{f}_{n_1, m}(r_1) \int r_2 dr_2 \tilde{f}_{n'_2, m'}(r_2) \tilde{f}_{n_2, m}(r_2) \bar{V}_{|m-m'|}^{sc}(r_1, r_2), \end{aligned} \quad (\text{B.3})$$

where

$$\bar{V}_{|m-m'|}^{sc}(r_1, r_2) = \int_0^\pi \frac{d\phi}{\pi} \cos(|m-m'|\phi) \tilde{V}^{sc}(\sqrt{r_1^2 + r_2^2 - 2r_1 r_2 \cos \phi}). \quad (\text{B.4})$$

It should be noted that the potential $\tilde{V}^{sc}(r_{12})$ contains a $1/r_{12}$ singular term in the bare-potential part, which diverges as $r_1 \rightarrow r_2$. Thus, care must be exercised when performing the real-space integration. We rewrite the integral over r_1 and r_2 in Eq. (B.4) as

$$\begin{aligned} &\int r_1 dr_1 \tilde{f}_{n'_1, m'}(r_1) \tilde{f}_{n_1, m}(r_1) \int r_2 dr_2 \tilde{f}_{n'_2, m'}(r_2) \tilde{f}_{n_2, m}(r_2) \bar{V}_{|m-m'|}^{sc}(r_1, r_2) \\ &= \int r_> dr_> \int_0^{r_>} r_< dr_< \left[\tilde{f}_{n'_1, m'}(r_>) \tilde{f}_{n_1, m}(r_>) \tilde{f}_{n'_2, m'}(r_<) \tilde{f}_{n_2, m}(r_<) \right. \\ &\quad \left. + \tilde{f}_{n'_1, m'}(r_<) \tilde{f}_{n_1, m}(r_<) \tilde{f}_{n'_2, m'}(r_>) \tilde{f}_{n_2, m}(r_>) \right] \bar{V}_{|m-m'|}^{sc}(r_<, r_>) \\ &= \int r_>^3 dr_> \int_0^1 p dp \left[\tilde{f}_{n'_1, m'}(r_>) \tilde{f}_{n_1, m}(r_>) \tilde{f}_{n'_2, m'}(p r_>) \tilde{f}_{n_2, m}(p r_>) \right. \\ &\quad \left. + \tilde{f}_{n'_1, m'}(p r_>) \tilde{f}_{n_1, m}(p r_>) \tilde{f}_{n'_2, m'}(r_>) \tilde{f}_{n_2, m}(r_>) \right] \bar{V}_{|m-m'|}^{sc}(r_>, p r_>), \end{aligned} \quad (\text{B.5})$$

where $r_> = \max(r_1, r_2)$ and $r_< = \min(r_1, r_2)$. For the singular part of $\tilde{V}^{sc}(r_{12})$, the angular integration given in Eq. (B.4) reduces to elliptic functions of the ratio $p = r_</r_>$.

In the limit $k_F \rightarrow 0$, we have

$$\begin{aligned} \lim_{k_F \rightarrow 0} \langle n'_1, n'_2, m' | V_{e_1 e_2} | n_1, n_2, m \rangle &= \frac{4\pi^2 e^2}{\epsilon_{sc}} C_{n'_1, m'} C_{n'_2, m'} C_{n_1, m} C_{n_2, m} \\ &\times \int dq I_{2-\delta_{m,0}-\delta_{m'},0}^{(m-m')}(\alpha_{n'_1} + \alpha_{n_1}, q) I_{2-\delta_{m,0}-\delta_{m'},0}^{(m-m')}(\alpha_{n'_2} + \alpha_{n_2}, q). \end{aligned} \quad (\text{B.6})$$

Appendix III. RESOLUTION OF EQ. (23)

• Polarized Fermi sea

We first project $(H - E_i^{(eeh)})|\Psi_i^{(eeh)}\rangle = 0$ into the exciton state $|\Psi_{j'}^{(e)}\rangle$ with $m = 0$. This leads to

$$\begin{aligned} (E_{j'}^{(e)} - E_i^{(eeh)})z_{X,j'}^{(i)} + \sum_j \sum_{\mathbf{q},\ell} \langle \Psi_{j'}^{(e)} | H a_{\mathbf{q},\frac{1}{2}} | \Psi_j^{(ee)} \rangle G_{\ell,0}(q) z_{T,j,\ell}^{(i)} \\ + \sum_{n_1, n_2, \ell, m_1, m_3} \langle \Psi_{j'}^{(e)} | H | n_1, n_2, \ell, m_1, m_3, 1/2 \rangle z_{n_1, n_2, \ell, m_1, m_3, \frac{1}{2}}^{(i)} = 0, \end{aligned} \quad (\text{C.1})$$

where $E_{j'}^{(e)}$ are exciton eigen-energies. The second term describes the coupling between the exciton and the trion-hole states (including bound and unbound states) that is induced by Coulomb interaction. Here, \mathbf{q} and \mathbf{q}' are restricted in the spin-(1/2) Fermi sea, $|F_{N_+}\rangle$. We have

$$\begin{aligned} \langle \Psi_{j'}^{(e)} | H a_{\mathbf{q},\frac{1}{2}} | \Psi_j^{(ee)} \rangle = \sum_{n_1, n_2, n'_1, m} x_{n'_1,0}^{(j')} t_{n_1, n_2, m}^{(j)} \sum_{\mathbf{k}_2} \phi_{n_2, -m}(\mathbf{k}_2) \\ \times \left[\sum_{\mathbf{k}'_1, \mathbf{k}_1} \phi_{n'_1,0}^*(\mathbf{k}'_1) \phi_{n_1, m}(\mathbf{k}_1) v_{ee}(\mathbf{k}_1, \mathbf{k}_2; \mathbf{k}'_1, \mathbf{q}) - \delta_{m,0} O_{n_1, n'_1}^{(0)} V(\mathbf{k}_2 - \mathbf{q}) \right], \end{aligned} \quad (\text{C.2})$$

where the term $v_{ee}(\mathbf{k}_1, \mathbf{k}_2; \mathbf{k}'_1, \mathbf{q})$ comes from the Coulomb interaction between the electron e_1 with spin $(-1/2)$ in the exciton and the FS electron e_2 with spin $(1/2)$; the term $V(\mathbf{k}_2 - \mathbf{q})$ comes from the scattering of the FS electron e_2 by the Coulomb interaction with the valence hole.

The matrix elements are more efficiently evaluated in real-space integrals. We have

$$\begin{aligned} \sum_{\mathbf{q}, \ell, 0} \langle \Psi_{j'}^{(e)} | H a_{\mathbf{q},\frac{1}{2}} | \Psi_j^{(ee)} \rangle G_{\ell,0}(q) = \sum_{n_1, n_2, n'_1, m} x_{n'_1,0}^{(j')} t_{n_1, n_2, m}^{(j)} \left[C_{n'_1,0} C_{n_1, m} C_{n_2, m} \right. \\ \left. \times \int d\mathbf{r}_1 \tilde{f}_{n'_1,0}(r_1) \tilde{f}_{n_1, m}(r_1) \int d\mathbf{r}_2 \tilde{f}_{n_2, m}(r_2) Q_{\ell,0}(r_2) \bar{V}_{|m|}^{sc}(r_1, r_2) + \delta_{m,0} O_{n'_1, n_1} \langle n_2, 0 | \tilde{V}_{eh} | \ell, 0 \rangle \right], \end{aligned} \quad (\text{C.3})$$

where

$$\langle n'_2, m | \tilde{V}_{eh} | \ell, m \rangle = -C_{n'_2, m} \int d\mathbf{r} \tilde{f}_{n'_2, m}(r) Q_{\ell, m}(r) \tilde{V}^{sc}(r), \quad (\text{C.4})$$

and

$$Q_{\ell, m}(r) = \frac{i^m}{2\pi} \int_0^{k_F} q dq G_{\ell,0}(q) J_m(qr). \quad (\text{C.5})$$

For the third term in Eq. (C.1), we have

$$\begin{aligned} \langle \Psi_{j'}^{(e)} | H | n_1, n_2, \ell, m_1, m_3, 1/2 \rangle = \sum_{n'_1} x_{n'_1,0}^{(j')} C_{n'_1,0} C_{n_1, m_1} C_{n_2, m_2} \\ \times 4\pi^2 \int r_1 dr_1 \tilde{f}_{n'_1,0}(r_1) \tilde{f}_{n_1, m_1}(r_1) \int r_2 dr_2 \tilde{f}_{n_2, m_2}(r_2) Q_{\ell, m_3}(r_2) \bar{V}_{|m_1|}^{sc}(r_1, r_2) \\ + \delta_{m_1,0} \sum_{n'_1} x_{n'_1,0}^{(j')} O_{n'_1, n_1}^{(0)} \langle n_2, m_3 | \tilde{V}_{eh} | \ell, m_3 \rangle, \end{aligned} \quad (\text{C.6})$$

where $m_2 = -(m_1 + m_3)$. We next project the Schrödinger equation for $|\Psi_i^{(eeh)}\rangle$ into the trion-FS hole basis state $G_{\ell',0}(q') a_{\mathbf{q}'_1, \frac{1}{2}} | \Psi_{j'}^{(ee)} \rangle$. This gives

$$\begin{aligned} \sum_{\mathbf{q}'} G_{\ell',0}(q') \langle \Psi_j^{(ee)} | a_{\mathbf{q}', \frac{1}{2}}^\dagger H | \Psi_j^{(e)} \rangle z_{X,j}^{(i)} + \sum_{j,\ell} \sum_{\mathbf{q}', \mathbf{q}} G_{\ell',0}(q') \langle \Psi_j^{(ee)} | a_{\mathbf{q}', \frac{1}{2}}^\dagger (H - E_i^{(eeh)}) a_{\mathbf{q}, \frac{1}{2}} | \Psi_j^{(ee)} \rangle G_{\ell,0}(q) z_{T,j,\ell}^{(i)} \\ + \sum_{m_3 \neq 0} \sum_{n_1, n_2, \ell, m_1} \sum_{\mathbf{q}'} G_{\ell',0}(q') \langle \Psi_j^{(ee)} | a_{\mathbf{q}', \frac{1}{2}}^\dagger H | n_1, n_2, \ell, m_1, m_3, \frac{1}{2} \rangle z_{n_1, n_2, \ell, m_1, m_3, \frac{1}{2}}^{(i)} = 0. \end{aligned} \quad (\text{C.7})$$

where it is understood that the sums over \mathbf{q} and \mathbf{q}' are restricted inside the FS due to the cut-off function included in $G_{\ell,0}(q)$. The matrix elements in the first term of the above equation are written explicitly as

$$\begin{aligned} \sum_{\mathbf{q}'\mathbf{q}} G_{\ell',0}(q') \langle \Psi_j^{(ee)} | a_{\mathbf{q}',\frac{1}{2}}^\dagger (H - E_i^{(eeh)}) a_{\mathbf{q},\frac{1}{2}} | \Psi_j^{(ee)} \rangle G_{\ell,0}(q) = \\ \left[(E_j^{(ee)} - E_i^{(eeh)}) \delta_{\ell',\ell} - \tilde{K}_{\ell',\ell} + \sum_{\mathbf{q},\mathbf{q}'} G_{\ell',0}(q') V(\mathbf{q}' - \mathbf{q}) G_{\ell,0}(q) \right] \delta_{j',j} \\ - \sum_{n_1, n_2, m} t_{n_1', n_2', m}^{(j')} t_{n_1, n_2, m}^{(j)} \sum_{\mathbf{q}'\mathbf{q}} G_{\ell',0}(q') \left[O_{n_2', n_2}^{(m)} \sum_{\mathbf{k}_1', \mathbf{k}_1} \phi_{n', m}^*(\mathbf{k}_1') \phi_{n, m}(\mathbf{k}_1) v_{ee}(\mathbf{k}_1', \mathbf{q}; \mathbf{k}_1, \mathbf{q}') \right. \\ \left. + O_{n_1', n_1}^{(m)} \sum_{\mathbf{k}_2', \mathbf{k}_2} \phi_{n_2', -m}^*(\mathbf{k}_2') \phi_{n_2, -m}(\mathbf{k}_2) (v_{ee}(\mathbf{k}_2', \mathbf{q}; \mathbf{k}_2, \mathbf{q}') - v_{ee}(\mathbf{k}_2', \mathbf{q}; \mathbf{q}', \mathbf{k}_2)) \right] G_{\ell,0}(q), \end{aligned} \quad (\text{C.8})$$

where $E_j^{(ee)}$ is the j trion-state energy.

On the RHS of the above equation, the first term describes the energy for the trion part. The second term contains the kinetic-energy matrix elements for the FS hole defined by

$$\tilde{K}_{\ell',\ell} = \frac{1}{2\pi} \int_0^{k_F} q^3 dq G_{\ell',0}(q) G_{\ell,0}(q), \quad (\text{C.9})$$

which can be carried out analytically and we have $\tilde{K}_{\ell,\ell} = k_F^2(1/3 - 1/(2\ell\pi)^2)$ and $\tilde{K}_{\ell',\ell} = (k_F/\pi)^2 [1/(\ell' - \ell)^2 - 1/(\ell + \ell')^2] (-1)^{\ell+\ell'}$ for $\ell' \neq \ell$. The third term is the Coulomb interaction between the valence hole and the FS hole, which is repulsive, whose matrix elements are simply

$$\langle \ell', 0 | V_{eh} | \ell, 0 \rangle = \sum_{\mathbf{q}, \mathbf{q}'} G_{\ell',0}(q') V(\mathbf{q}' - \mathbf{q}) G_{\ell,0}(q) = \frac{1}{4\pi^2} \int_0^{k_F} q' dq' \int_0^{k_F} q dq G_{\ell',0}(q') \tilde{V}_0^{sc}(q', q) G_{\ell,0}(q), \quad (\text{C.10})$$

where

$$\tilde{V}_m^{sc}(q', q) = \int_0^\pi \frac{d\phi}{\pi} \cos(m\phi) \frac{2\pi e^2}{\epsilon_{sc} q (1 + qr_0) \kappa_q} \Big|_{q=\sqrt{q_1^2 + q_2^2 - 2q_1 q_2 \cos\phi}}. \quad (\text{C.11})$$

The fourth term contains the Coulomb interaction between the spin-(1/2) electron of the trion and the FS hole, and finally the direct and exchange Coulomb interactions between the spin-(1/2) electron of the trion and the FS hole.

The explicit matrix elements for direct Coulomb scattering between electron and FS-hole are

$$\begin{aligned} \sum_{\mathbf{k}_2', \mathbf{k}_2, \mathbf{q}', \mathbf{q}} G_{\ell',0}(q') \phi_{n_2', -m}^*(\mathbf{k}_2') v_{ee}(\mathbf{k}_2', \mathbf{q}; \mathbf{k}_2, \mathbf{q}') \phi_{n_2, -m}(\mathbf{k}_2) G_{\ell,0}(q) \\ = C_{n_2', m} C_{n_2, m} 4\pi^2 \int r_2 dr_2 \int r_3 dr_3 \tilde{f}_{n_2', m}(r_2) \tilde{f}_{n_2, m}(r_2) \bar{V}_0^{sc}(r_2, r_3) Q_{\ell', 0}(r_3) Q_{\ell, 0}(r_3), \end{aligned} \quad (\text{C.12})$$

and for the exchange Coulomb scattering

$$\begin{aligned} \sum_{\mathbf{k}_2', \mathbf{k}_2, \mathbf{q}', \mathbf{q}} G_{\ell',0}(q') \phi_{n_2', -m}^*(\mathbf{k}_2') \phi_{n_2, -m}(\mathbf{k}_2) v_{ee}(\mathbf{k}_2', \mathbf{q}; \mathbf{q}', \mathbf{k}_2) G_{\ell,0}(q) \\ = C_{n_2', m} C_{n_2, m} 4\pi^2 \int r_2 dr_2 \int r_3 dr_3 \tilde{f}_{n_2', m}(r_2) Q_{\ell', 0}(r_3) \bar{V}_{|m|}^{sc}(r_2, r_3) Q_{\ell, 0}(r_2) \tilde{f}_{n_2, m}(r_3). \end{aligned} \quad (\text{C.13})$$

Similarly, the matrix elements for the coupling between trion-hole states and the $m_3 \neq 0$ basis states are given by

$$\begin{aligned} \sum_{\mathbf{q}'} G_{\ell',0}(q') \langle \Psi_j^{(ee)} | a_{\mathbf{q}',\frac{1}{2}}^\dagger H | n_1, n_2, \ell, m_1, m_3, \frac{1}{2} \rangle \\ = - \sum_{n_1', n_2', \ell'} t_{n_1', n_2', m_2}^{(j)} O_{n_2', n_2}^{(m_2)} C_{n_1', m_2} C_{n_1, m_1} \int d\mathbf{r}_1 \int d\mathbf{r}_3 \tilde{f}_{n_1', m_2}(r_1) Q_{\ell', 0}(r_3) \bar{V}_{|m_3|}^{sc}(r_1, r_3) \tilde{f}_{n_1, m_1}(r_1) Q_{\ell, m_3}(r_3) \\ - \sum_{n_1', n_2', \ell'} t_{n_1', n_2', m_1}^{(j)} O_{n_1', n_1}^{(m_1)} C_{n_2', m_1} C_{n_2, m_2} \left[\int d\mathbf{r}_2 \int d\mathbf{r}_3 \tilde{f}_{n_2', m_1}(r_2) Q_{\ell', 0}(r_3) \bar{V}_{|m_3|}^{sc}(r_2, r_3) \tilde{f}_{n_2, m_2}(r_2) Q_{\ell, m_3}(r_3) \right. \\ \left. - \int d\mathbf{r}_2 \int d\mathbf{r}_3 \tilde{f}_{n_2', m_1}(r_2) Q_{\ell, m_3}(r_2) \bar{V}_{|m_2|}^{sc}(r_2, r_3) Q_{\ell', 0}(r_3) \tilde{f}_{n_2, m_2}(r_3) \right] \Big|_{m_2 = -m_1 - m_3}. \end{aligned} \quad (\text{C.14})$$

Finally, we project the Schrödinger equation for $|\Psi_i^{(eeh)}\rangle$ into the $m_3 \neq 0$ basis states. We obtain for the diagonal block associated with $m_3 \neq 0$ basis states

$$\begin{aligned}
\langle n'_1, n'_2, \ell', m'_1, m'_3, \frac{1}{2} | H | n_1, n_2, \ell, m_1, m_3, \frac{1}{2} \rangle &= \delta_{m'_1, m_1} \delta_{m'_3, m_3} \left\{ [K_{n'_1, n_1}^{(m_1)} + \langle n'_1, m_1 | \tilde{V}_{eh} | n_1, m_1 \rangle] O_{n'_2, n_2}^{(m_2)} \delta_{\ell', \ell} \right. \\
&+ O_{n'_1, n_1}^{(m_1)} [K_{n'_2, n_2}^{(m_2)} + \langle n'_2, m_2 | \tilde{V}_{eh} | n_2, m_2 \rangle] \delta_{\ell', \ell} + O_{n'_1, n_1}^{(m_1)} O_{n'_2, n_2}^{(m_2)} [-\tilde{K}_{\ell', \ell} + \langle \ell', m_3 | V_{eh} | \ell, m_3 \rangle] \left. \right\} \\
&+ \delta_{m'_3, m_3} \delta_{\ell', \ell} C_{n'_1, m'_1} C_{n'_2, m'_2} C_{n_1, m_1} C_{n_2, m_2} \\
&\times \int d\mathbf{r}_1 \tilde{f}_{n'_1, m'_1}(r_1) \tilde{f}_{n_1, m_1}(r_1) \int d\mathbf{r}_2 \tilde{f}_{n'_2, m'_2}(r_2) \tilde{f}_{n_2, m_2}(r_2) \bar{V}_{|m_1 - m'_1|}^{sc}(r_1, r_2) \\
&- \delta_{m'_2, m_2} O_{n'_2, n_2}^{(m_2)} C_{n'_1, m'_1} C_{n_1, m_1} \int d\mathbf{r}_1 \int d\mathbf{r}_3 \tilde{f}_{n'_1, m'_1}(r_1) Q_{\ell', m'_3}(r_3) \bar{V}_{|m'_3 - m_3|}^{sc}(r_1, r_3) \tilde{f}_{n_1, m_1}(r_1) Q_{\ell, m_3}(r_3) \\
&- \delta_{m'_1, m_1} O_{n'_1, n_1}^{(m_1)} C_{n'_2, m'_2} C_{n_2, m_2} \left[\int d\mathbf{r}_2 \int d\mathbf{r}_3 \tilde{f}_{n'_2, m'_2}(r_2) Q_{\ell', m'_3}(r_3) \bar{V}_{|m'_3 - m_3|}^{sc}(r_2, r_3) \tilde{f}_{n_2, m_2}(r_2) Q_{\ell, m_3}(r_3) \right. \\
&\left. - \int d\mathbf{r}_2 \int d\mathbf{r}_3 \tilde{f}_{n'_2, m'_2}(r_2) Q_{\ell, m_3}(r_2) \bar{V}_{|m_2 + m'_3|}^{sc}(r_2, r_3) Q_{\ell', m'_3}(r_3) \tilde{f}_{n_2, m_2}(r_3) \right], \tag{C.15}
\end{aligned}$$

where $m_2 = -(m_1 + m_3)$, $m'_2 = -(m'_1 + m'_3)$, and

$$\langle \ell', m_3 | V_{eh} | \ell, m_3 \rangle = \int d\mathbf{r} Q_{\ell', m_3}(r) Q_{\ell, m_3}(r) \tilde{V}^{sc}(r). \tag{C.16}$$

$\langle \ell', m_3 | V_{eh} | \ell, m_3 \rangle$ can also be evaluated in momentum space as in Eq. (C.10) but with $\tilde{V}_0^{sc}(q', q)$ replaced by $\tilde{V}_{m_3}^{sc}(q', q)$.

• Unpolarized Fermi sea

For unpolarized FS ($N_+ = N_- = N/2$), we must also add the contribution of the basis states $|n_1, n_2, \ell, m_1, m_3, -1/2\rangle$ for all possible single electron-hole pair excitations resulting in a spin- $(-1/2)$ FS hole. Here we have two electrons of the same spin above the Fermi surface. Thus, it is important to keep track on the anticommutation of the two-electron states. It is more convenient to use an orthogonal set of one-particle basis functions for both electrons (e1 and e2) via the Gram-Schmidt process. After the orthonormalization process, the basis states are denoted by $|\tilde{n}_1, \tilde{n}_2, \ell, m_1, m_3, -1/2\rangle$. We write the orthonormalized basis functions as

$$\langle \mathbf{r} | \tilde{n}, m \rangle = \tilde{g}_{\tilde{n}, m}(r) e^{im\varphi}. \tag{C.17}$$

Here we impose the constraint $\tilde{n}_1 < \tilde{n}_2$ for $m_1 = m_2$ in the basis set due to the Pauli exclusion principle. Since these basis states only couple to the exciton states with a frozen FS, the additional matrix elements are

$$\begin{aligned}
\langle \Psi_{j'}^{(e)} | H | \tilde{n}_1, \tilde{n}_2, \ell, m_1, m_3, -\frac{1}{2} \rangle &= \sum_{\tilde{n}'_1} x_{\tilde{n}'_1, 0}^{(j')} \left[\int d\mathbf{r}_1 \tilde{g}_{\tilde{n}'_1, 0}(r_1) \tilde{g}_{\tilde{n}_1, m_1}(r_1) \int d\mathbf{r}_2 \tilde{g}_{\tilde{n}_2, m_2}(r_2) Q_{\ell, m_3}(r_2) \bar{V}_{|m_1|}^{sc}(r_1, r_2) \right. \\
&- \int d\mathbf{r}_1 \tilde{g}_{\tilde{n}'_1, 0}(r_1) \tilde{g}_{\tilde{n}_2, m_2}(r_1) \int d\mathbf{r}_2 \tilde{g}_{\tilde{n}_1, m_1}(r_2) Q_{\ell, m_3}(r_2) \bar{V}_{|m_2|}^{sc}(r_1, r_2) \left. \right] \\
&+ \left[\delta_{m_1, 0} x_{\tilde{n}_1, 0}^{(j')} \langle \tilde{n}_2, m_3 | \tilde{V}_{eh} | \ell, m_3 \rangle - \delta_{m_2, 0} x_{\tilde{n}_2, 0}^{(j')} \langle \tilde{n}_1, m_3 | \tilde{V}_{eh} | \ell, m_3 \rangle \right] \tag{C.18}
\end{aligned}$$

and

$$\begin{aligned}
\langle \tilde{n}'_1, \tilde{n}'_2, \ell', m'_1, m'_3, -\frac{1}{2} | H | \tilde{n}_1, \tilde{n}_2, \ell, m_1, m_3, -\frac{1}{2} \rangle &= \delta_{m'_1, m_1} \delta_{m'_3, m_3} \left\{ [K_{\tilde{n}'_1, \tilde{n}'_1}^{(m_1)} + \langle \tilde{n}'_1, m_1 | \tilde{V}_{eh} | \tilde{n}_1, m_1 \rangle] \delta_{\tilde{n}'_2, \tilde{n}_2} \delta_{\ell', \ell} \right. \\
&+ \delta_{\tilde{n}'_1, \tilde{n}_1} [K_{\tilde{n}'_2, \tilde{n}'_2}^{(m_2)} + \langle \tilde{n}'_2, m_2 | \tilde{V}_{eh} | \tilde{n}_2, m_2 \rangle] \delta_{\ell', \ell} + \delta_{\tilde{n}'_1, \tilde{n}_1} \delta_{\tilde{n}'_2, \tilde{n}_2} [-\tilde{K}_{\ell', \ell} + \langle \ell', m_3 | \tilde{V}_{eh} | \ell, m_3 \rangle] \left. \right\} \\
&+ \delta_{m'_3, m_3} \delta_{\ell', \ell} \left[\int d\mathbf{r}_1 \tilde{g}_{\tilde{n}'_1, m'_1}(r_1) \tilde{g}_{\tilde{n}_1, m_1}(r_1) \int d\mathbf{r}_2 \tilde{g}_{\tilde{n}'_2, m'_2}(r_2) \tilde{g}_{\tilde{n}_2, m_2}(r_2) \bar{V}_{|m_1 - m'_1|}^{sc}(r_1, r_2) \right. \\
&\quad \left. - \int d\mathbf{r}_1 \tilde{g}_{\tilde{n}'_1, m'_1}(r_1) \tilde{f}_{\tilde{n}_2, m_2}(r_1) \int d\mathbf{r}_2 \tilde{g}_{\tilde{n}'_2, m'_2}(r_2) \tilde{f}_{\tilde{n}_1, m_1}(r_2) \bar{V}_{|m_2 - m'_1|}^{sc}(r_1, r_2) \right] \\
&- \delta_{m'_2, m_2} \delta_{n'_2, n_2} \left[\int d\mathbf{r}_1 \int d\mathbf{r}_3 \tilde{g}_{\tilde{n}'_1, m'_1}(r_1) Q_{\ell', m'_3}(r_3) \bar{V}_{|m'_3 - m_3|}^{sc}(r_1, r_3) \tilde{g}_{\tilde{n}_1, m_1}(r_1) Q_{\ell, m_3}(r_3) \right. \\
&\quad \left. - \int d\mathbf{r}_1 \int d\mathbf{r}_3 \tilde{g}_{\tilde{n}'_1, m'_1}(r_1) Q_{\ell', m'_3}(r_3) \bar{V}_{|m'_3 - m_1|}^{sc}(r_1, r_3) \tilde{g}_{\tilde{n}_1, m_1}(r_1) Q_{\ell, m_3}(r_1) \right] \\
&+ \delta_{m'_2, m_1} \delta_{\tilde{n}'_2, \tilde{n}_1} \left[\int d\mathbf{r}_1 \int d\mathbf{r}_3 \tilde{g}_{\tilde{n}'_1, m'_1}(r_1) Q_{\ell', m'_3}(r_3) \bar{V}_{|m'_3 - m_3|}^{sc}(r_1, r_3) \tilde{g}_{\tilde{n}_2, m_2}(r_1) Q_{\ell, m_3}(r_3) \right. \\
&\quad \left. - \int d\mathbf{r}_1 \int d\mathbf{r}_3 \tilde{g}_{\tilde{n}'_1, m'_1}(r_1) Q_{\ell', m'_3}(r_3) \bar{V}_{|m'_3 - m_2|}^{sc}(r_1, r_3) \tilde{g}_{\tilde{n}_2, m_2}(r_3) Q_{\ell, m_3}(r_1) \right] \\
&- \delta_{m'_1, m_1} \delta_{\tilde{n}'_1, \tilde{n}_1} \left[\int d\mathbf{r}_2 \int d\mathbf{r}_3 \tilde{g}_{\tilde{n}'_2, m'_2}(r_2) Q_{\ell', m'_3}(r_3) \bar{V}_{|m'_3 - m_3|}^{sc}(r_2, r_3) \tilde{g}_{\tilde{n}_2, m_2}(r_2) Q_{\ell, m_3}(r_3) \right. \\
&\quad \left. - \int d\mathbf{r}_2 \int d\mathbf{r}_3 \tilde{g}_{\tilde{n}'_2, m'_2}(r_2) Q_{\ell', m'_3}(r_3) \bar{V}_{|m'_3 - m_2|}^{sc}(r_2, r_3) Q_{\ell, m_3}(r_2) \tilde{g}_{\tilde{n}_2, m_2}(r_3) \right] \\
&+ \delta_{m'_1, m_2} \delta_{\tilde{n}'_1, \tilde{n}_2} \left[\int d\mathbf{r}_2 \int d\mathbf{r}_3 \tilde{g}_{\tilde{n}'_2, m'_2}(r_2) Q_{\ell', m'_3}(r_3) \bar{V}_{|m'_3 - m_3|}^{sc}(r_2, r_3) \tilde{g}_{\tilde{n}_1, m_1}(r_2) Q_{\ell, m_3}(r_3) \right. \\
&\quad \left. - \int d\mathbf{r}_2 \int d\mathbf{r}_3 \tilde{g}_{\tilde{n}'_2, m'_2}(r_2) Q_{\ell', m'_3}(r_3) \bar{V}_{|m'_3 - m_1|}^{sc}(r_2, r_3) Q_{\ell, m_3}(r_2) \tilde{g}_{\tilde{n}_1, m_1}(r_3) \right] \quad (C.19)
\end{aligned}$$

where $m'_2 = -(m'_1 + m'_3)$ and $m_2 = -(m_1 + m_3)$.

*yiachang@gate.sinica.edu.tw

-
- ¹ G.D. Mahan, Phys. Rev. **153**, 882 (1967).
 - ² S. Schmitt-Rink, C.Ell, and H. Haug, Phys. Rev. B **33**, 1183 (1986).
 - ³ G. D. Sanders and Y. C. Chang, Phys. Rev. B **35**, 1300 (1987), and references therein.
 - ⁴ S. Schmitt-Rink, D.S. Chemla, and D.A.B. Miller, Adv. Phys. **38**, 89 (1989).
 - ⁵ P.Hawrylak, Phys. Rev. B **44**, 3821 (1991).
 - ⁶ G.E.W. Bauer, Phys. Rev. B **45**, 9153 (1992).
 - ⁷ G. V. Astakhov, V. P. Kochereshko, D. R. Yakovlev, W. Ossau, J. Nurnberger, W. Faschinger, and G. Landwehr, Phys. Rev. B **62**, 10345 (2000).
 - ⁸ A. A. Klochikhin, V. P. Kochereshko, L. Besombes, G. Karczewski, T. Wojtowicz, and J. Kossut, Physica Status Solidi (c), **7(6)**, 1661 (2010).
 - ⁹ R. A. Suris, V.P. Kochereshko, G.V. Astakhov, D.R. Yakovlev, W. Ossau, J. Nrnberger, W. Faschinger, G. Landwehr, T. Wojtowicz, G. Karczewski, and J. Kossut, Phys. Stat. Sol. (b) **227(2)**, 343, (2001).
 - ¹⁰ R. A. Suris, in Optical Properties of 2D Systems with Interacting Electrons, edited by W. Ossau and R. A. Suris (NATO Scientific Series, Kluwer, 2003), p. 111; arXiv:1310.6120.
 - ¹¹ A. A. Klochikhin, V.P. Kochereshko, and S. Tatarenko, Journal of Luminescence **154**, 310 (2014).
 - ¹² A. V. Koudinov, C. Kehl, A. V. Rodina, J. Geurts, D. Wolverson, and G. Karczewski, Phys. Rev. Lett. **112**, 147402 (2014).
 - ¹³ S.-Y. Shiau, M. Combescot, and Y.-C. Chang, Europhys. Lett. **117**, 57001 (2017).
 - ¹⁴ D. K. Efimkin and A. H. MacDonald, Phys. Rev. B **95**, 035417 (2017).
 - ¹⁵ K. F. Mak, K. He, C. Lee, G. H. Lee, J. Hone, T. F. Heinz, and J. Shan, Nat. Mater. **12**, 207 (2013).
 - ¹⁶ M. Sidler, P. Back, O. Cotlet, A. Srivastava, T. Fink, M. Kroner, E. Demler, and A. Imamoglu, Nature Physics **13**, 255 (2017).
 - ¹⁷ Y. Lin, X. Ling, L. Yu, S. Huang, A. L. Hsu, Y.-H. Lee, J. Kong, M. S. Dresselhaus, and T. Palacios, Nano Lett. **14**, 5569 (2014).
 - ¹⁸ B. Ganchev, N. Drummond, I. Aleiner, and V. Fal'ko, Phys. Rev. Lett. **114**, 107401 (2015).
 - ¹⁹ E. Courtade, et al., Phys. Rev. B **96**, 085302 (2017).
 - ²⁰ M. Szyniszewski, E. Mostaani, N. D. Drummond, and V. I. Fal'ko, Phys. Rev. B **95**, 081301 (2017).
 - ²¹ G. Wang, et al., Rev. Mod. Phys. **90**, 021001 (2018) and

- references therein.
- ²² D. Y. Qiu, F. H. da Jornada, and S. G. Louie, *Phys. Rev. Lett.* **111**, 216805 (2013).
 - ²³ M. M. Ugeda et. al., *Nature Materials* **13**, 1091 (2014).
 - ²⁴ A. Chernikov, T. C. Berkelbach, H. M. Hill, A. Rigosi, Y. Li, O. B. Aslan, D. R. Reichman, M. S. Hybertsen, and T. F. Heinz, *Phys. Rev. Lett.* **113**, 076802 (2014).
 - ²⁵ K. Hao, J. F. Specht, P. Nagler, L. Xu, K. Tran, A. Singh, C. K. Dass, C. Scholler, T. Korn, M. Richter, A. Knorr, X. Li, G. Moody, *Nature Commun.* **8**, 15552 (2017).
 - ²⁶ J. S. Ross, S. Wu, H. Yu, N. J. Ghimire, A. M. Jones, G. Aivazian, J. Yan, D. G. Mandrus, D. Xiao, W. Yao et al., *Nat. Commun.* **4**, 1474 (2013).
 - ²⁷ A. M. Jones, H. Yu, N. J. Ghimire, S. Wu, G. Aivazian, J. S. Ross, B. Zhao, J. Yan, D. G. Mandrus, D. Xiao et al., *Nat. Nanotechnol.* **8**, 634 (2013).
 - ²⁸ A. Singh, G. Moody, S. Wu, Y. Wu, N. J. Ghimire, J. Yan, D. G. Mandrus, X. Xu, and X. Li, *Phys. Rev. Lett.* **112**, 216804 (2014).
 - ²⁹ H. J. Liu, L. Jiao, L. Xie, F. Yang, J. L. Chen, W. K. Ho, C. L. Gao, J. F. Jia, X. D. Cui, and M. H. Xie, *2D Mater.* **2**, 034004 (2015).
 - ³⁰ B. Zhu, X. Chen, and X. Cui, *Sci. Rep.* **5**, 9218 (2015).
 - ³¹ J. Yang, T. Lu, Y. W. Myint, J. Pei, D. Macdonald, J.-C. Zheng, and Y. Lu, *ACS Nano* **9**, 6603 (2015).
 - ³² W. Ritz, *Journal fur die Reine und Angewandte Mathematik* **135**, 1 (1909).
 - ³³ J. K. MacDonald, *Phys. Rev.* **43** 830 (1933).
 - ³⁴ L. V. Keldysh, *JETP Lett.* **29**, 658 (1979).
 - ³⁵ F. Stern, *Phys. Rev. Lett.* **18**, 546 (1967).
 - ³⁶ G. Strinati, *Phys. Rev. B* **29**, 5718 (1984).
 - ³⁷ B. Stébé and A. Ainane, *Superlattices and Microstructures* **5**, 545 (1989).
 - ³⁸ A. Thilagam, *Phys. Rev. B* **55**, 7804 (1997).
 - ³⁹ R. A. Sergeev and R. A. Suris, *Nanotechnology* **12**, 597 (2001).
 - ⁴⁰ X. L. Yang, S. H. Guo, F. T. Chan, K. W. Wong, W. Y. Ching, *Phys. Rev. A* **43**, 1186 (1991).